CHAPTER-IV

Mixed ligand molybdenum complexes of 2-pivaloylamino-6-acetonylisoxanthopterin (H_2L^2) and suitable ancillary ligands.

Abstract

In this chapter the redox reaction between $Na_2MoO_4.2H_2O$ and 2-pivaloylamino-6-acetonylisoxanthopterin (H_2L^2) [Scheme (IV-1)] has been studied in the presence of selected ancillary ligands like 8-hydroxyquinoline [H(ox)], 2-marcaptobenzoic acid [H_2(mba)] and sodium diethyldithiocarbamate [Na(dedtc)].$3H_2O$ [Scheme (IV-2)]. This effort led to the isolation of three new Mo(IV) complexes **(1)** to **(3)** in the pure form. Further reaction of compound **(3)** with Me_3NO afforded another new di-μ-oxo bridged Mo(V) complex. All these four complexes have been characterized through elemental analysis, different spectral data like ESIMS, IR, UV-VIS, fluorescence and ^{1}H-NMR (1D and 2D) as well as cyclic voltammetry. The reativities of compounds **(1)** to **(3)** towards Me_3NO have been studied using UV-VIS spectroscopy. The isolation of compound **(4)** from compound **(3)** points towards the oxygen atom transfer (OAT) nature of the reaction involving the Mo(IV) center of the reactant complex.

Introduction

Pterins (2-amino-4-oxopteridines) are important in a wide range of biological functions including a large number of metal-containing enzymes (e.g., Fe, Mo, [33,91,103]. The redox non-innocent nature of the pterin ring is associated with the ability of its pyrazine ring to exist in a number of oxidation states [70]. In the above enzymes, this redox capability of the pterin moiety is matched by the ability of the metal centers to display multiple oxidation states [34]. This aspect has catalyzed research work on the coordination chemistry of pteridines in general and pterins in particular [34,49,93,94]. Literature survey reveals the existence of only a limited amount of data on the synthetic molybdenum- pterin complexes [4e] and provides with the impetus for the present endeavour using 2-pivaloylamino-6-acetonylisoxanthopterin (H_2L^2) [Scheme (IV-1)]. Its 1″-pivaloyl group plays a crucial role in enhancing solubility of the unsubstituted pterin and facilitating the synthetic and purification steps [5a,75]. Here (H_2L^2) acts as a reducing agent towards the Mo(VI) starting material $Na_2MoO_4.2H_2O$ leading to the formation of the present Mo(IV) complexes **(1)**, **(2)**, **(3)** and **(4)**. Their characterization aspects, spectroscopic analysis and reactivity studies towards a biologically relevant substrate (Me_3NO) is delineated here [5b,13a,104,105]. For establishing the reaction stoichiometry, the

product [compound **(4)**] of the reaction of one of the complexes with Me_3NO has been isolated in the solid state and characterized.

Attempt have been made to touch upon all the biologically important oxidation state of molybdenum (IV, V and VI) here, utilizing the redox non-innocent pterin ligand H_2L^2 [Scheme (IV-1)].

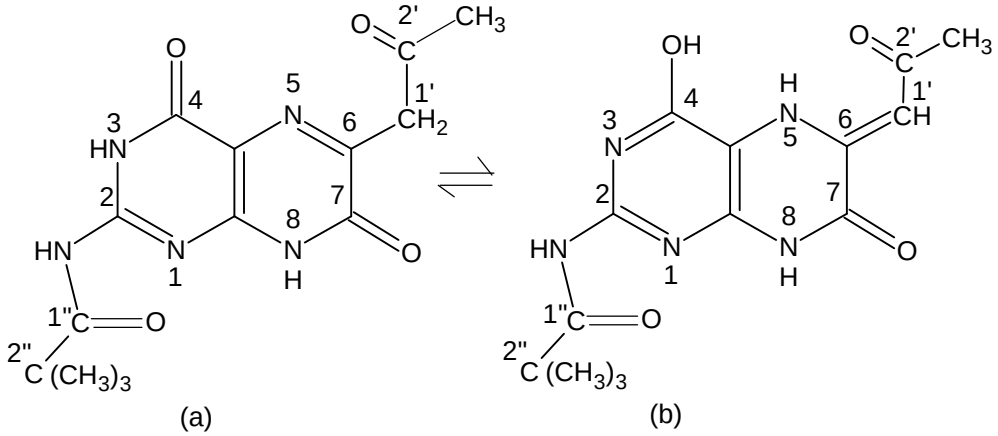

Scheme (IV-1): Structural formulae of the two tautomeric forms of the free of pterin ligand (H_2L^2)

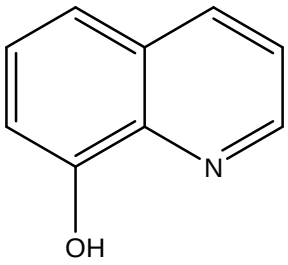

8-Hydroxyquinoline [H(ox), C_9H_7NO, F.W. 145.16]

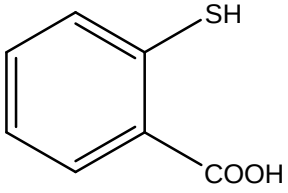

2-Mercaptobenzoic acid [H_2(mba), $C_6H_7S_2O$, F.W. 154.19]

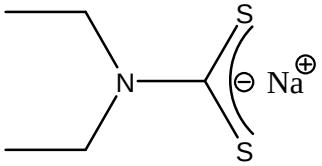

Sodium diethyldithiocarbamate [Na(dedtc).$3H_2O$, $C_5H_{17}NS_2O_3Na$, F.W. 208.27]

Scheme (IV-2)

Experimental

Materials

Most of the materials used are mentioned in the CHAPTER-III under the same heading.

Method

Here also all the compounds were synthesized under darkness, dinitrogen atmosphere and controlled heating in a paraffin oil bath using Schlenk procedure [Fig. (III-1) and Fig. (III-2)]. All the solvents used were dried to remove moisture at the desired limit [2].

Synthesis

2-pivaloylamino-6-acetonylisoxantho pterin (H_2L^2)

Preparation of this ligand is stated in CHAPTER-III.

$[Mo^{IV}(ox)_2 (L^2)].CH_3OH$ (1)

To an aqueous solution (5 mL) of $Na_2MoO_4.2H_2O$ (0.1 g, 0.40 mmol) a methanolic solution of 2-pivaloylamino-6-acetonylisoxanthopterin (H_2L^2, 0.25 g, 0.78 mmol) was added in a three-neck round-bottomed flask, pH of this solution was adjusted to 5.2 by 1:3 HCl and refluxed (paraffin oil bath) under boiling at 345K for 6h under darkness and dinitrogen atmosphere. Solvent was dried by a rotary evaporator. After redissolving the residue in CH_3OH, 8-hydroxyquinoline [H(ox), 0.06g, 0.41 mmol] was added to it. It was stirred at 300K for 2h under darkness and dinitrogen atmosphere. Solvent was again evaporated by a rotary evaporator. The crude product obtained subjected to flash chromatography (silica gel 230 – 400 mesh) for purification using CH_2Cl_2: CH_3OH (95.5 v/v) as eluant. Final yellow brown product was obtained by removing the solvent in a rotary evaporator and dried over P_4O_{10} in vacuo. Yield was 70%. Purity was checked through TLC (UV lamp). [Found C, 54.5; H, 4.10; N, 13.40 %; MoC_{33} $H_{31}O_7N_7$ (733.59), C, 54.03; H, 4.26; N, 13.37 %]. UV-VIS (CH_3OH) λ_{max}/mm (log ε) 218 (4.96), 241 (4.95), 281sh (4.48), 307sh (4.36), 346 (4.51), 370sh (4.38), 413 (4.33) and 441sh (4.09). Schematic structure of compound **(1)** is shown in Scheme (IV-3).

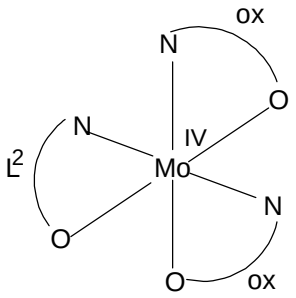

Scheme (IV-3)

$(PPh_4)_2$ $[Mo^{IV}(mba)_2$ $(L^2)].CH_3OH$ (2)

A methanolic solution (60 ml) of 2-pivaloylamino-6-acetnonylisoxanthopterin (H_2L^2, 0.25 g, 0.78 mmol) and an aqueous solution (10 ml) of $Na_2MoO_4.2H_2O$ (0.1 g, 0.4 mmol) were mixed and pH was adjusted to 5.42 by 1:3 HCl. The mixture was refluxed (paraffin oil bath) under boiling at 345K for 6h under dinitrogen atmosphere and darkness. The reddish brown product thus obtained was dried in a rotary evaporator. Redissolving it in CH_3OH (60 ml), 2-mercaptobenzoic acid [H_2(mba), 0.07 g, 0.45 mmol] was added to it. After stirring for 15 min, tetraphenylphosphonium bromide (PPh_4Br, 0.434 g, 1.04 mmol) was added. Then the mixture was stirred at 303K under dinitrogen atmosphere and darkness for 2h. After evaporating the solvent in a rotary evaporator, the compound was purified by flask chromatography (silica gel 230 – 400 mesh) using CH_2Cl_2: CH_3OH (95:5 v/v) as eluant; the deep brown compound thus obtained was dried over P_4O_{10} in vacuo. Yield was 65%. [Found C, 64.30; H, 4.7; N, 5.09 %; $MoC_{77}H_{69}N_5O_9S_2P_2$ (1430.43) calcd, C, 64.66; H, 4.86; N, 4.90 %]. UV-VIS (CH_3OH) λ_{max}/mm (log ε): 223sh (5.07), 277sh (4.38), 346 (4.11), 418sh (3.86) and 449sh (3.66). Schematic structure of compound **(2)** is shown in Scheme (IV-4).

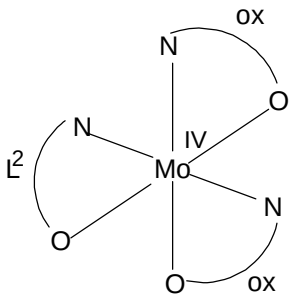

Scheme (IV-4)

$[Mo^{IV}(dedtc)\ (L^2)^{2-}(HL^2)^{1-}].CH_3OH$ (3)

An aqueous solution (5 mL) of $Na_2MoO_4.2H_2O$ (0.1 g, 0.40 mmol) was treated with a methanolic solution (60 ml) of 2-pivaloylamino-6-acetonylisoxanthopterin (H_2L^2, 0.3 g, 0.94 mmol) and pH was adjusted to 5.34 by 1:3 HCl solution; the mixture was refluxed (paraffin oil bath) under boiling at 345K under darkness and dinitrogen atmosphere for 6h. Resulting solution was dried in a rotary evaporator. After redissolving the compound in CH_3OH sodium diethyldithiocarbonate [$Na(dedtc).3H_2O$, 0.068 gm, 0.40 mmol] was added and reaction was carried out at 313K for 2h under darkness and dinitrogen atmosphere. After removing the solvent in a rotary evaporator the crude product was purified by flash chromatography (silica gel 230 – 400 mesh) and the eluant was CH_2Cl_2:CH_3OH (95:5 v/v). The final snuff coloured product was obtained by evaporating the solvent in a rotary evaporator and dried over P_4O_{10} in vacuum. Yield was 60%. Purity was checked through TLC (UV lamp). [Found C, 44.90; H, 4.86; N, 17.01 % ($MoC_{34}H_{45}N_{11}O_9S_2$) (911.86), calcd, C, 44.78, H, 4.97; N, 16.90 %]. UV-VIS (CH_3OH) λ_{max}/nm (log ε), 219 (4.86), 242sh (4.52), 285sh (4.39), 345.5 (4.39), 413.5 (4.26) and 443.0sh (4.09). Schematic structure of compound **(3)** is shown in Scheme (IV-5).

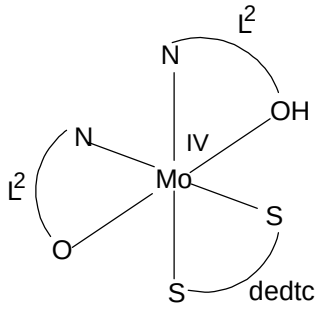

Scheme (IV-5)

$[(OCH_3)(L^2)Mo^V\mu(O_2)MoV(dedtc)(L^2)].CH_3OH$ (4)

A solution (65 ml) of compound **(3)** (0.3 g, 0.33 mmol) in CH_3OH was added to $Me_3N{\rightarrow}O$ (0.024 g, 0.33 mmol) solution (20 ml). The mixture was kept overnight at 301K with mild stirring under darkness and dinitrogen atmosphere. Then it was dried in a rotary evaporator and subjected to flash chromatography (silica gel 230-400 mesh) for purification. Eluting solvent was CH_2Cl_2:CH_3OH (92:8 v/v). Final dark brown product was obtained by evaporating the solvent in a rotary evaporator and dried in vacuum over P_4O_{10}. Yield was 55%. Purity was checked through TLC (UV-lamp). [Found C, 39.24; H, 4.19; N, 14.80 %; $Mo_2C_{35}H_{47}N_{11}O_{12}S_2$ (1069.82) calcd, C, 39.29; H, 4.43; N, 14.40 %]. UV-VIS (CH_3OH) λ_{max}/nm (log ε), 217 (5.08),

248.5sh (4.80), 288.5 (4.75), 347 (4.69), 421sh (4.35) and 448 sh (4.17). Schematic structure of compound **(4)** as well as the probable reaction pathway is shown in Scheme (IV-6).

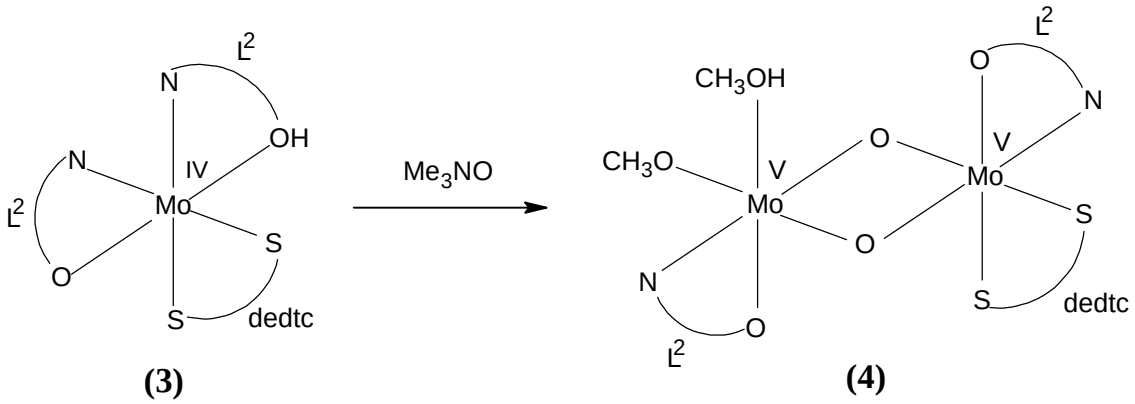

(3) **(4)**

Scheme (IV-6)

Results and Discussion
ESIMS data

The ESIMS data of pterin ligand (H_2L^2) are represented in Fig. (III-3) to Fig. (III-6).

The molecular ion peak (most abundant isotopic mass) obtained at the m/z (=703) region in the ESIMS spectra of the compound **(1)** is presented in the Fig. (IV-1a). The peak may be assigned as $[M + 2H]^+$ or $[MoC_{32}H_{29}O_6N_7]^+$, where M represents the desolvated species of this compound. Sometimes the [M + 2] isotopic peak is prominent due to the presence of O, F, P and I in the corresponding compound [11]. The theoretical distribution pattern is presented in the Fig. (IV-1b). It represents the architectural stability as well as compactness of the coordination core.

Fig. (IV-2a) represents the ESIMS data of compound **(2)** at the m/z (=713.65) region. The peak (most abundant isotopic mass) may be assigned as $[M – (2PPh_4 + 3H)]^+$ or $[MoC_{28}H_{20}N_5O_8S_2]^+$, where M represents the desolvated species. Simulation of the peak is represented in the Fig. (IV-2b).

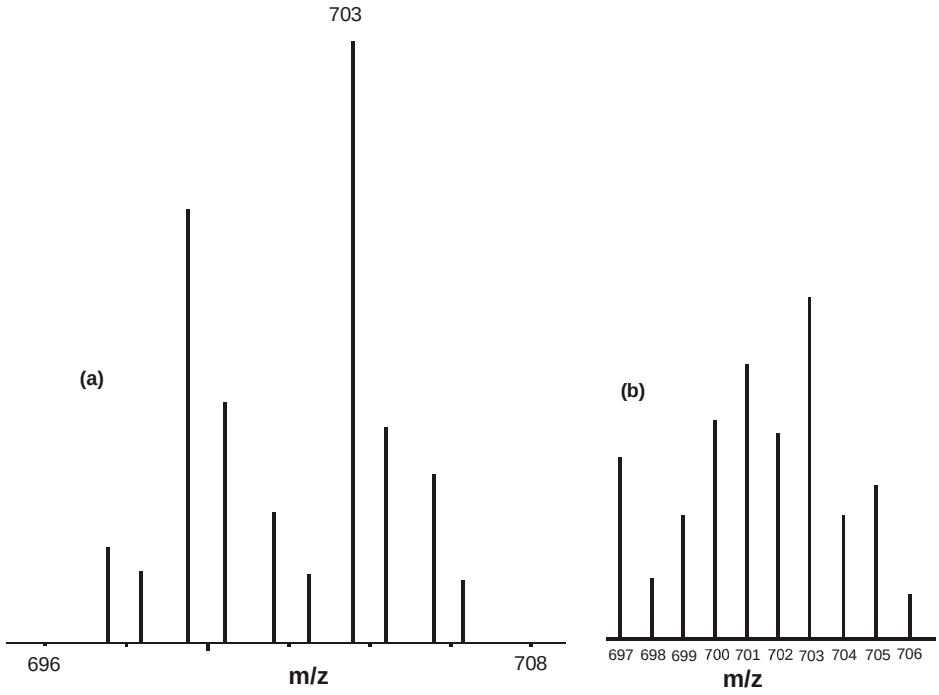

Fig. (IV-1): (a) ESIMS data of the compound **(1)** at the m/z(=703) region corresponding to the fragment $[M + 2H]^+$ or $[MoC_{32}H_{29}O_6N_7]^+$and (b) the calculated isotope pattern.

The stability of the compound **(3)** can be revealed from the ESIMS spectra of this compound. A molecular ion peak (most abundant isotopic mass) at the m/z (=879) region is obtained and shown in Fig. (IV-3a). It may be designated as $[M]^+$ or $[MoC_{33}H_{41}N_{11}O_8S_2]^+$, M is the desolvated species. The theoretical isotope distribution pattern is presented in the Fig. (IV-3b). The tally of the experimental isotope distribution pattern to that of calculated value proves the compactness of the core, conferred most likely by the $(dedtc)^{1-}$ ligand.

ESIMS spectrum of the compound **(4)** shows a peak (most abundant isotopic mass) at the m/z (= 987) region [Fig. (IV-4a)]. It may be assigned as $[M - (H_2O + CH_3OH)]^+$ or $[Mo_2C_{33}H_{37}N_{11}O_9S_2]^+$, where M represents the desolvated species. The theoretical calculated distribution pattern is shown in the Fig. (IV-4b). The difference in distribution pattern may be due to the ion-molecular interaction.

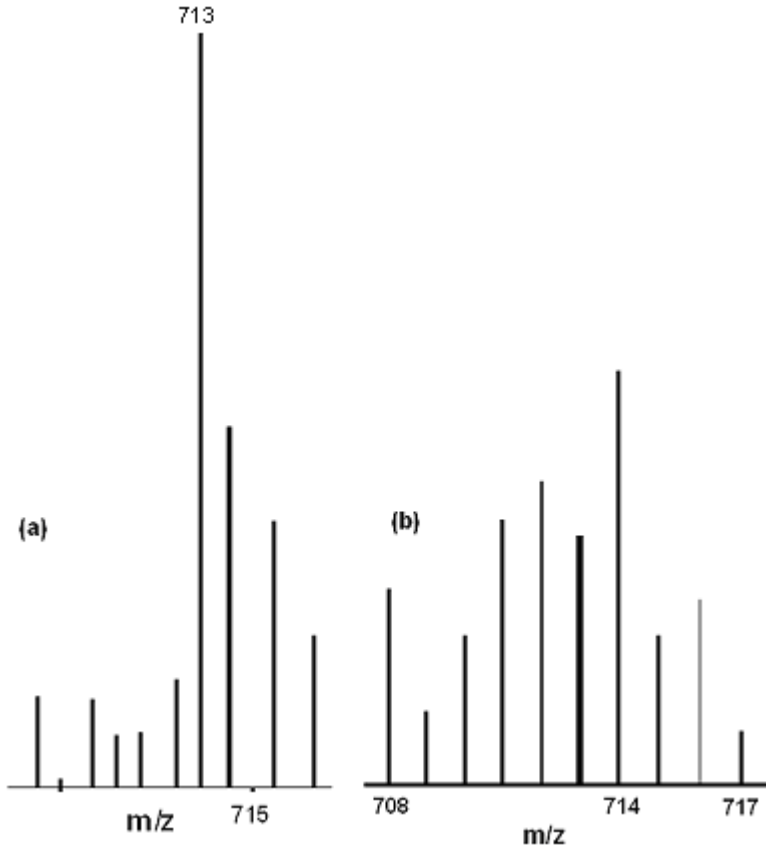

Fig. (IV-2): (a) ESIMS data of the compound **(2)** at the m/z(=713.65) region corresponding to the fragment $[M - (2PPh_4+3H)]^+$ or $[MoC_{28}H_{20}N_5O_8S_2]^+$ and (b) the calculated isotope pattern.

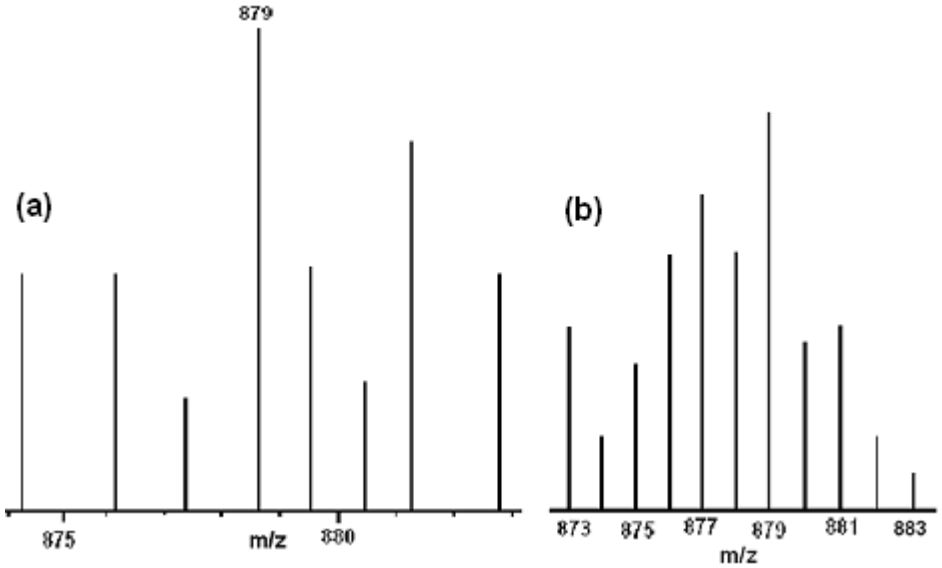

Fig. (IV-3): (a) ESIMS data of the compound **(3)** at the m/z(=879) region corresponding to the fragment $[M]^+$ or $[MoC_{33}H_{41}N_{11}O_8S_2]^+$ and (b) the calculated isotope pattern.

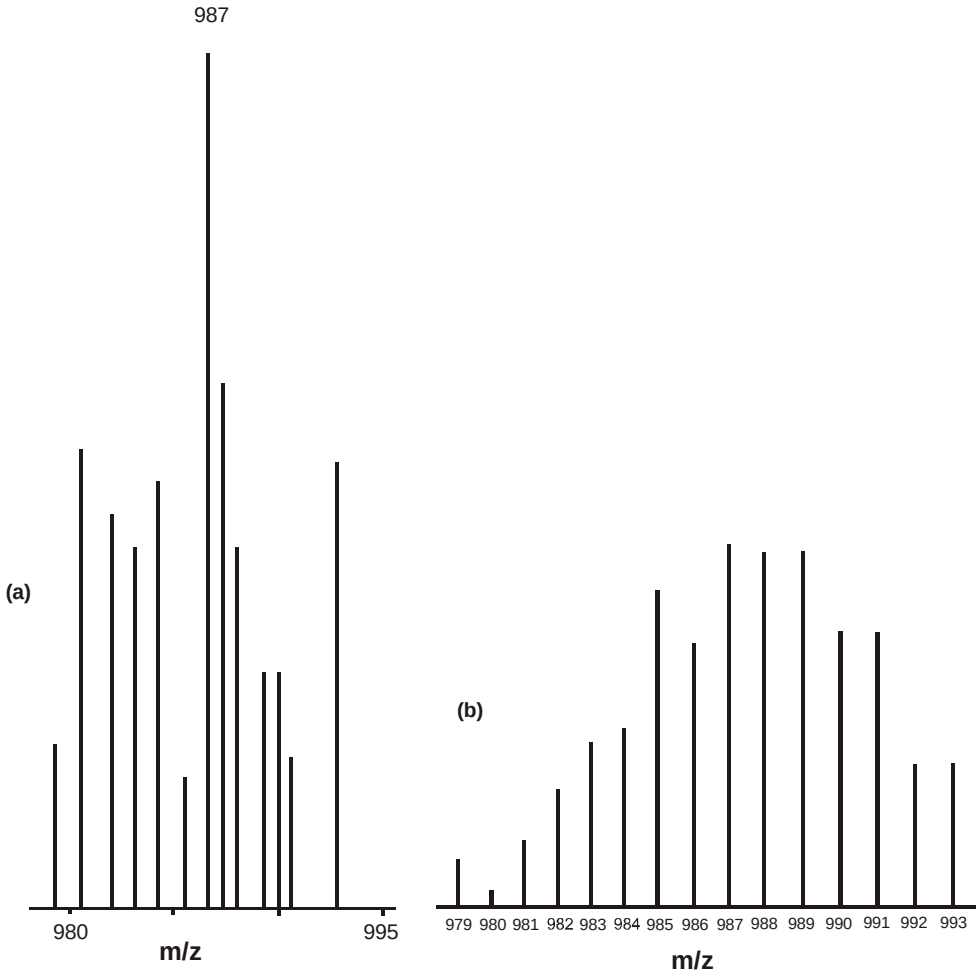

Fig. (IV-4): (a) ESIMS data of the compound **(4)** at the m/z(= 987) region corresponding to the fragment $[M - (H_2O + CH_3OH)]^+$ or $[Mo_2C_{33}H_{37}N_{11}O_9S_2]^+$ and (b) the calculated isotope pattern.

The foregoing observation of ESIMS data of these complexes can be summarized in the Table (IV-1).

Table (IV-1): The prominent ESIMS peaks (m/z) observed for compounds **(1)** to **(4)** along with their assignments, [Fig. (IV-1) to Fig. (IV-4)].

Compound	m/z	Assigned fragmentation peak observed in the ESIMS data*
(H_2L^2)	292.2	$[M - HCN]^+$;
(1)	703	$[M + 2H]^+$
(2)	713.65	$[M – (2PPh_4+3H)]^+$
(3)	879	$[M]^+$
(4)	987	$[M – (H_2O + CH_3OH)]^+$

IR spectrosopy

For the free pterin ligand (H_2L^2), the δ(OH) mode and δ(OH) + ν(C – O) mode appear at 1363.6 and 1328 cm^{-1} respectively. In all these compounds both these two bands are absent indicating deprotonation of the OH(4) functional group. The new ν(C – O) mode of the corresponding phenoxide group appears in the region 1103 – 1153 cm^{-1} for these compounds [Fig. (IV-5) to (IV-8)]. Most likely contribution from the ancillary ligands is responsible for the observed variation in the position of the ν(C – O) mode (1103 – 1153 cm^{-1}). The ligand anion resulting from tautomerism/deprotonation of H_2L^2 [Scheme (IV-1)] is shown in Scheme (IV-7), indicating bidentate O(4), N(5) coordination mode. The bands in the region 1660 to 1450 cm^{-1} [due to ν(C = O), ν(C – N), ν(C = N) and δ(N – H) modes] of the free ligand (H_2L^2) undergo changes both in shape and intensity in all these complexes due to electronic redistribution/ deprotonation/ tautomerism [Scheme (IV-7)] during the complex formation process. Changes of the relevant geometric parameters as obtained from the CHEM3D models [Table (IV-4), (IV-6), (IV-8) and (IV-10)] supports this view. For compounds **(1)** to **(3)** no prominent band appear in the region 990 – 800 cm^{-1} region, assignable to the ν(Mo=O_t) as well as ν(Mo – O_b – Mo) modes; this is consistent with their chemical composition indicating the absence the terminal and bridging oxygen atom. Only in case of compound **(4)** a prominent band appears at 802.3 cm^{-1}, indicating the presence of bridging Mo – O_b – Mo bonds [Scheme (IV-6)]

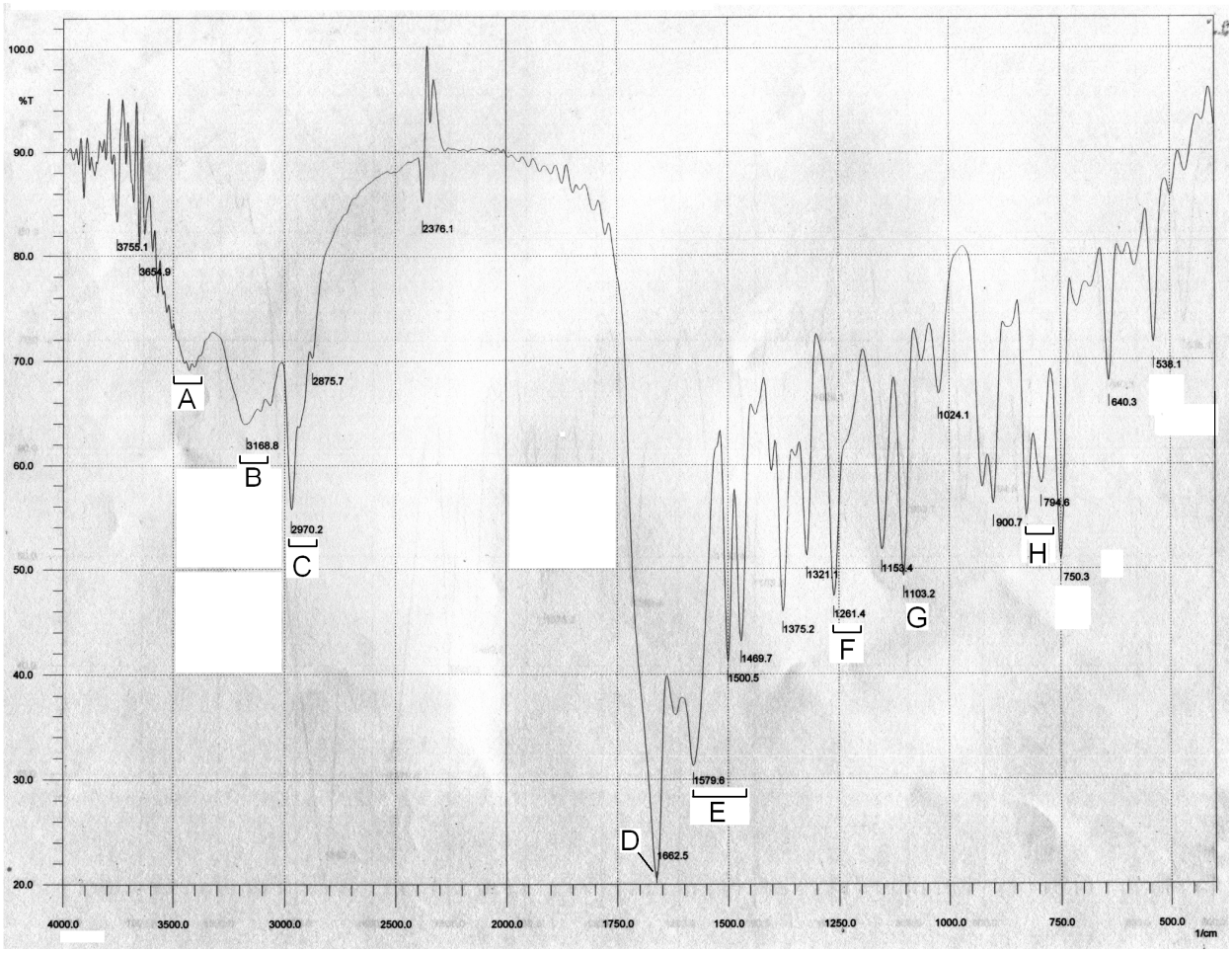

Fig. (IV-5): FTIR spectrum (KBr) of compound **(1)**

A: the broad O-H stretching vibration, hydrogen bonded (CH_3OH), 3423 cm^{-1}.

B: the broad N-H stretching vibration, hydrogen bonded, 3168 cm^{-1}.

C: the C-H stretching vibrations 2970, , 2875 cm^{-1}.

D: the C=O stretching vibrations of the (C=O) (1′) and (C=O) (2′) groups, 1662 cm^{-1}.

E: the C⋯C and C⋯N ring stretching vibrations of the pterin, $(ox)^{1-}$ 1579, 1500, 1469 cm^{-1}.

F: the ν (C-N) + δ (NH_2) vibrations , a broad band over the region 1200-1159 cm^{-1} [11].

G: the ν (C-O) mode of the O(4) phenoxide group, 1103 cm^{-1}.

H: the out-of-plane C-H (aromatic) bending vibrations, 794 cm^{-1}.

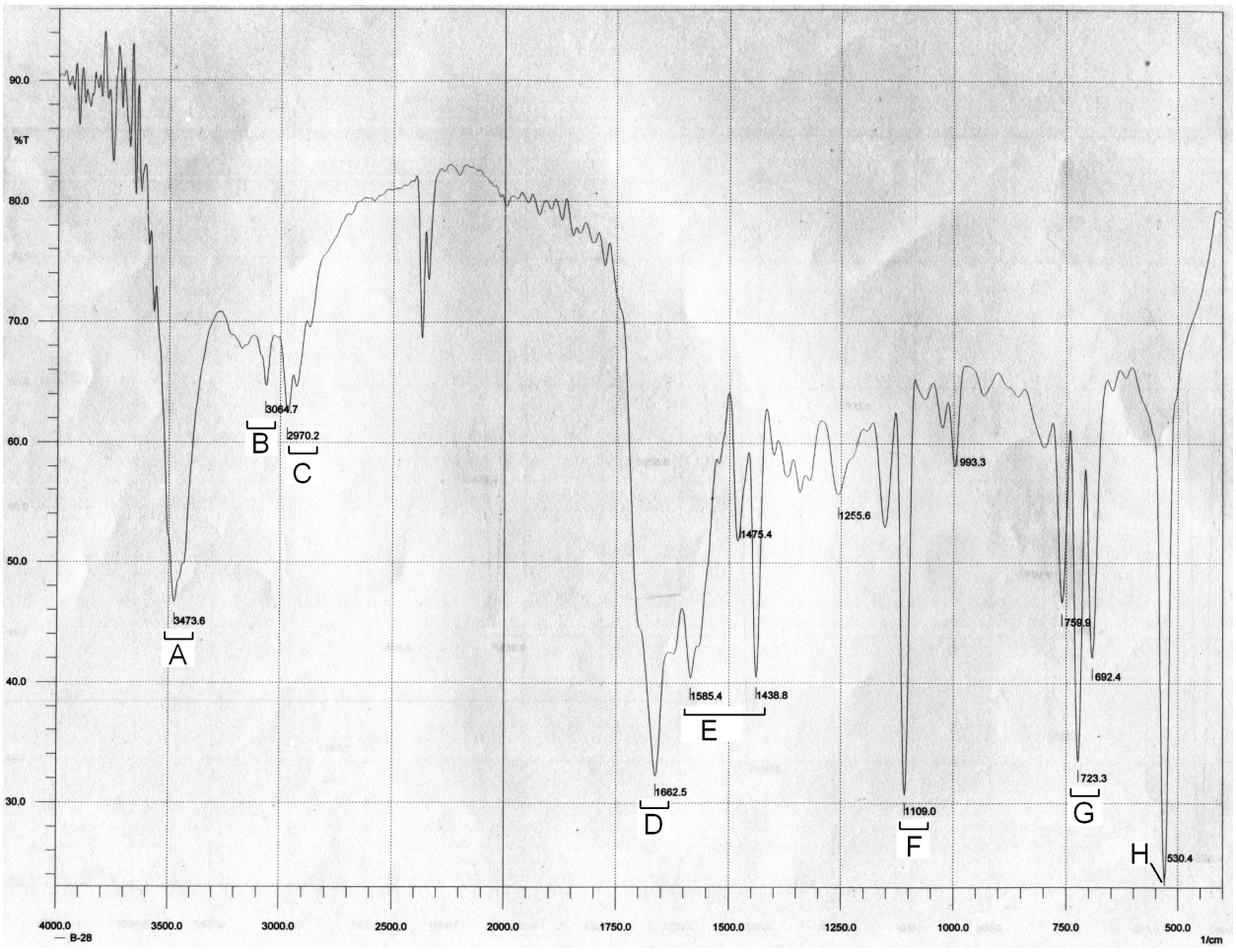

Fig. (IV-6): FTIR spectrum (KBr) of compound **(2)**

A: the broad O-H stretching vibration, hydrogen bonded (CH_3OH) 3473 cm^{-1}.
B: the broad N-H stretching vibration, hydrogen bonded, 3064 cm^{-1}.
C: the C-H stretching vibration, 2970 cm^{-1}.
D: the C=O stretching vibrations of the (C=O) (1′) and (C=O) (2′) groups, 1662 cm^{-1}.
E: the C⋯C and C⋯N ring stretching vibrations of the pterin, 1585, 1438 cm^{-1}.
F: the ν (C-O) mode of the O(4) phenoxide group, 1109 cm^{-1}.
G: the out-of-plane C-H (aromatic) bending vibrations, 723 cm^{-1} $(mba)^{2-}$.
H: the out-of-plane C⋯C (aromatic, Ph_4P^+) bending vibrations, 530 cm^{-1}.

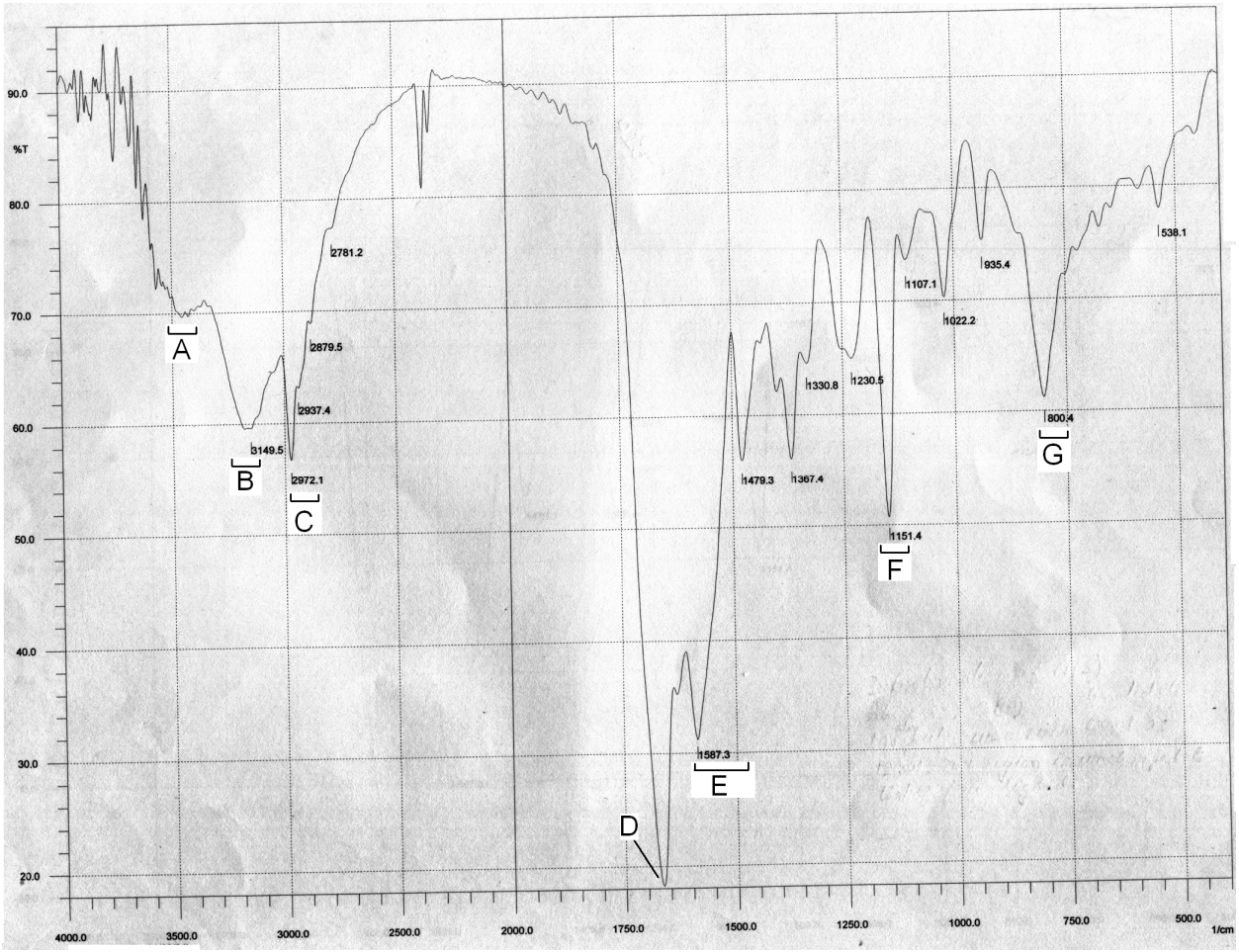

Fig. (IV-7): FTIR spectrum (KBr) of compound **(3)**

A: the broad O-H stretching vibration, hydrogen bonded (CH_3OH), 3423 cm^{-1}.
B: the broad N-H stretching vibration, hydrogen bonded, 3149 cm^{-1}.
C: the C-H stretching vibrations 2972, 2937, 2879 cm^{-1}.
D: the C=O stretching vibrations of the (C=O) (1′) and (C=O) (2′) groups, 1662 cm^{-1}.
E: the C⋯C and C⋯N ring stretching vibrations of the pterin, 1587, 1479 cm^{-1}.
F: the ν (C-O) mode of the O(4) phenoxide group, 1151 cm^{-1}.
G: the out-of-plane C-H (aromatic) bending vibrations, 800.4 cm^{-1}.

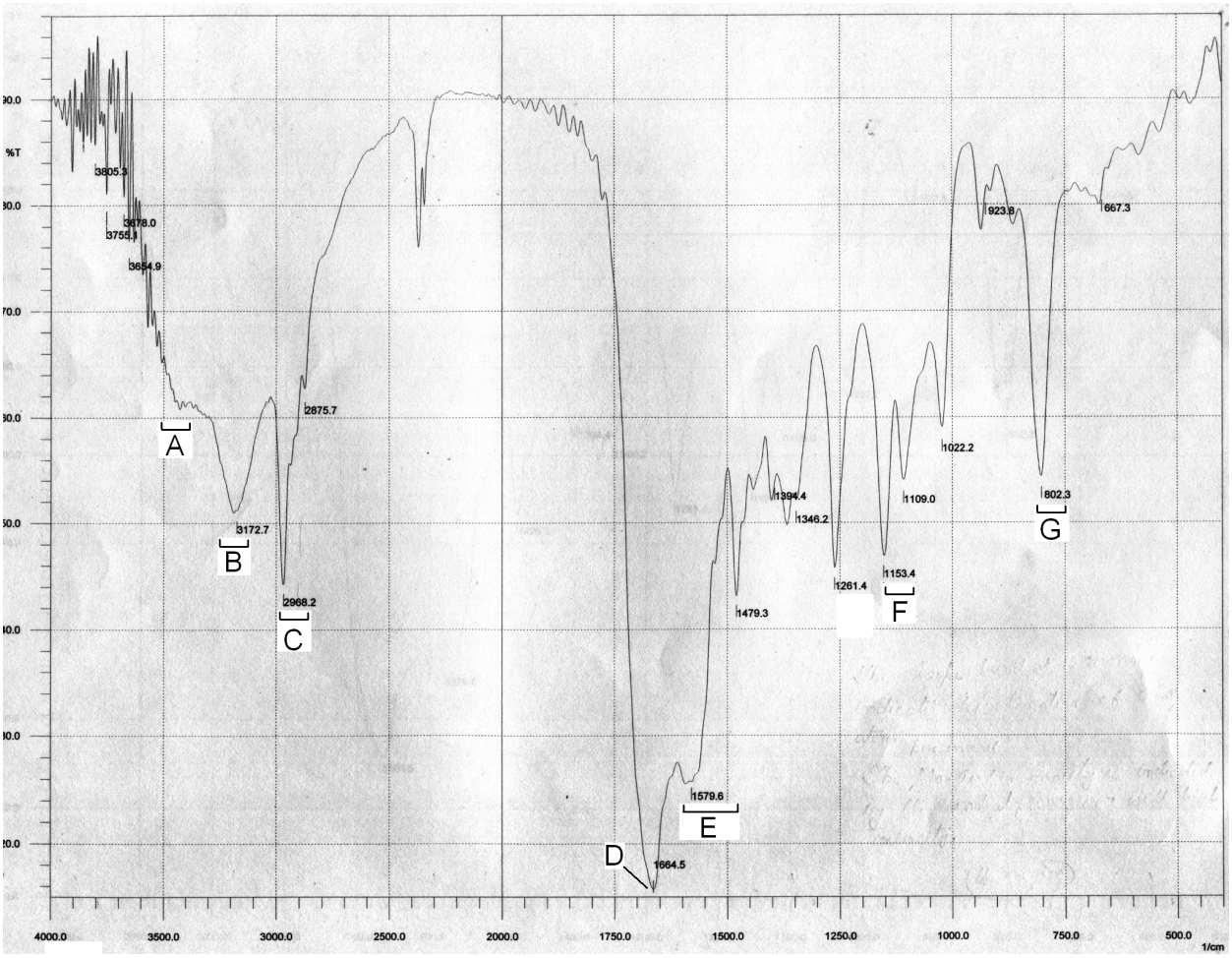

Fig. (IV-8): FTIR spectrum (KBr) of compound **(4)**

A: the broad O-H stretching vibration, hydrogen bonded (CH_3OH), 3423 cm^{-1}.
B: the broad N-H stretching vibration, hydrogen bonded, 3172 cm^{-1}.
C: the C-H stretching vibrations 2968, 2875 cm^{-1}.
D: the C=O stretching vibrations of the (C=O) (1′) and (C=O) (2′) groups, 1664 cm^{-1}.
E: the C⋯C and C⋯N ring stretching vibrations of the pterin, 1579, 1479 cm^{-1}.
F: the ν (C-O) mode of the O(4) phenoxide group, 1153 cm^{-1}.
G: the (Mo-O_b-Mo) stretching vibration at 802.3 cm^{-1} with increased intensity and modification compared with compound **(3)** [Fig. (IV-7)]

^{1}H-NMR spectroscopy

The 1-D and 2-D ^{1}H-NMR data of 8-hydroxyquinoline [H(ox)], are shown in Fig. (IV-9) and Fig. (IV-10) respectively. The quinoline ring proton signals could be assigned over region δ7.1- δ8.8 as supported by the corresponding 2D NMR data.

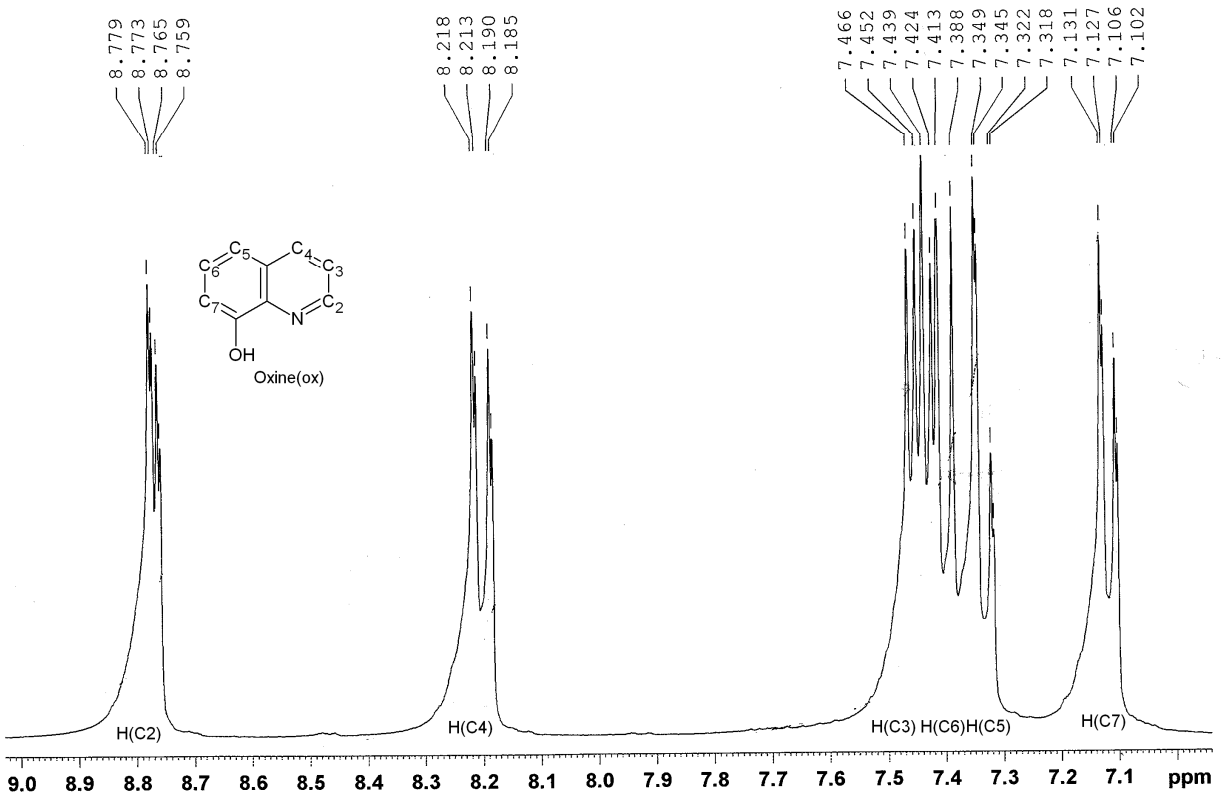

Fig.(IV-9): ^{1}H NMR data of H(ox) in DMSO-d_6 over the region δ9.0-7.0.

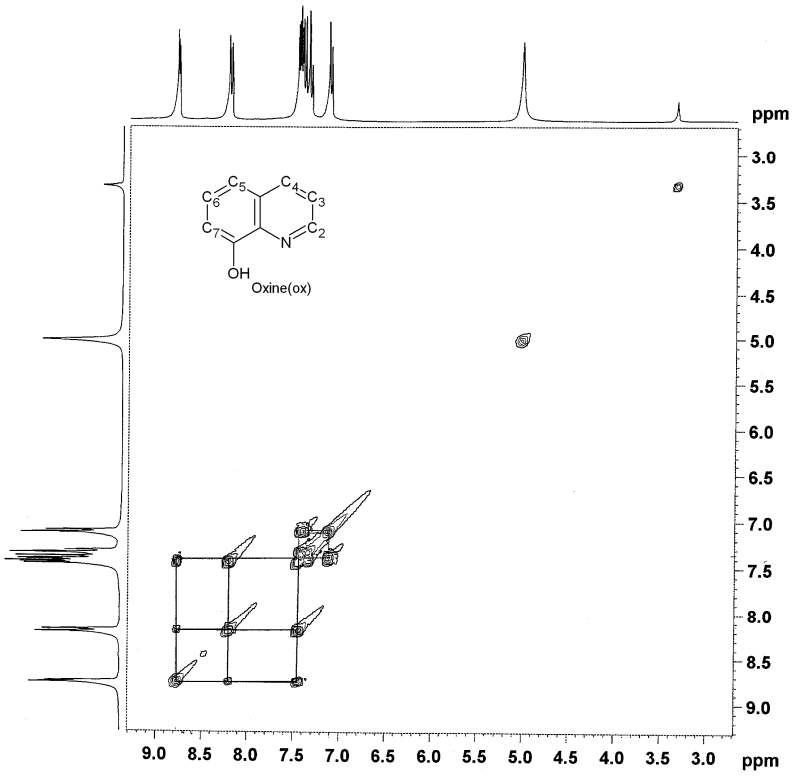

Fig. (IV-10): ^{1}H-^{1}H COSY data (symmetrized) of H(ox) in DMSO-d_6 over the region δ9.0-3.0.

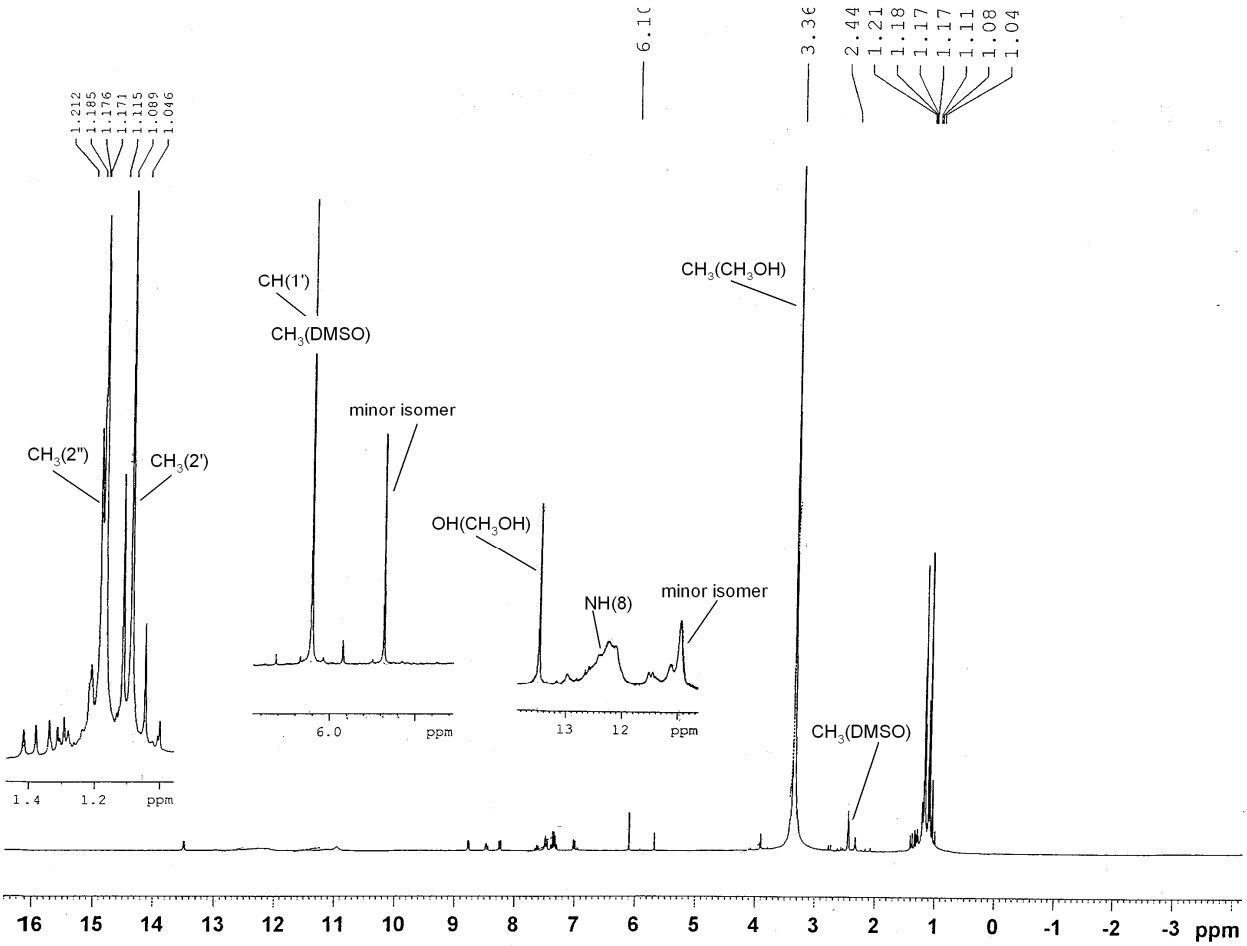

Fig. (IV-11): ^{1}H NMR data of compound **(1)** in DMSO-d_6 over the region δ16.0-0.0 (vide text for details).

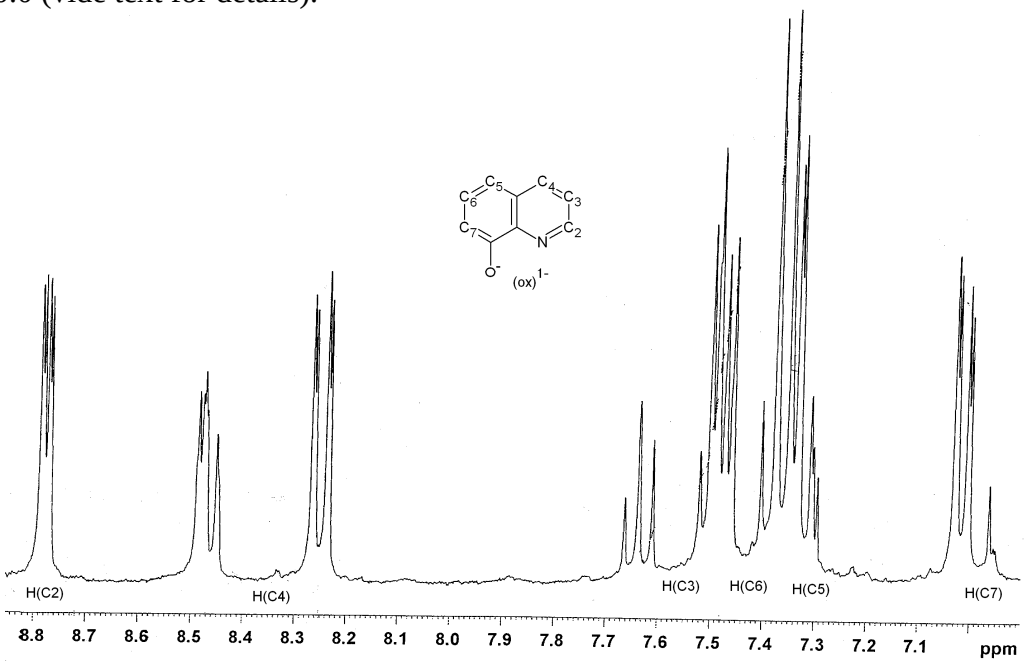

Fig. (IV-12): ^{1}H NMR data of compound **(1)** in DMSO-d_6 over the region δ8.8-7.0(vide text for details).

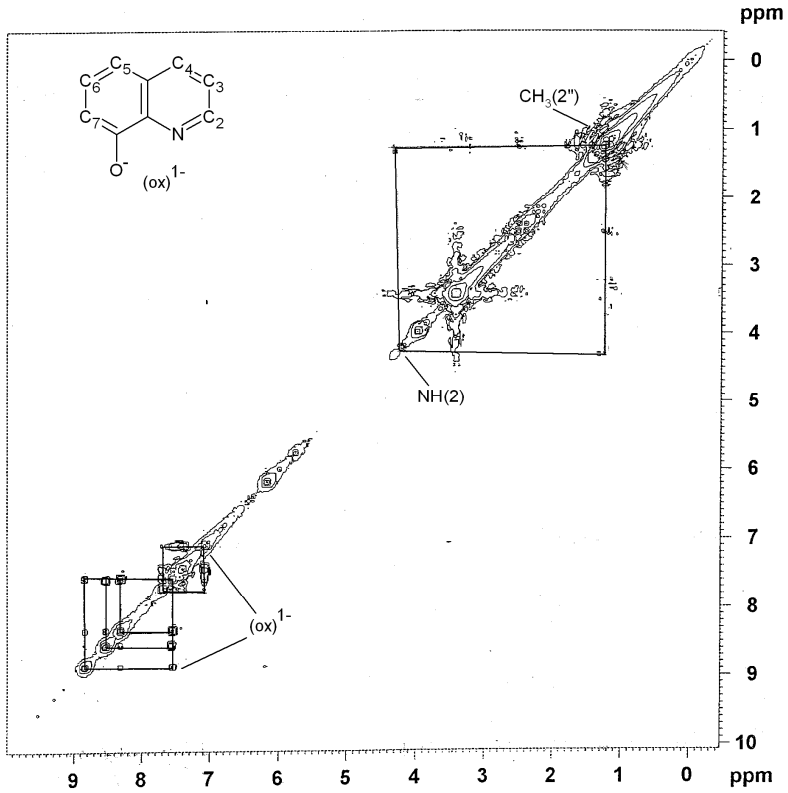

Fig. (IV-13): ^{1}H-^{1}H COSY data (symmetrized) of compound **(1)** in DMSO-d_6 over the region δ9.0-0.0 (vide text for details).

Fig. (IV-11) to Fig. (IV-13) represent the 1-D and 2-D NMR data of compound **(1)**. From the 1-D and 2-D NMR data the proton signals of the ancillary ligand $(ox)^{1-}$ could be located over the region δ7.0- δ8.8[Fig. (IV-12) and Fig. (IV-13)]. The chemical shift region of the quinoline ring protons remains essentially unchanged through metal coordination. However a change over in the splitting pattern of some of these signals is observed in the compound **(1)**; besides this, some of these signals are represented by more than one chemical shift values, indicating the difference between the two $(ox)^{1-}$ residues on the NMR time sale.

The OH(CH_3OH) and NH(8) signals could be located at δ13.52 and δ12.52 respectively. The CH(1′) signal is observed at δ6.12(ss), which is essentially unchanged with respect to that of the free pterin ligand (H_2L^2) (vide CHAPTER-III), indicating the bidentate nature of pterin ligand during the complex formation process, O(4) and N(5) atoms are utilized in the coordination process, leaving the carbonyl oxygen atom [-C=O(6)] free [Scheme (IV-1)]. 2-D NMR data help to locate the NH(2) and CH_3(2″) signals at δ4.15 and δ1.18. Now a closer observation of the proton signals over the relevant region help to locate the CH_3(2′) signal at δ1.11. Both these CH_3 signals are distorted doublet. Contributions from a minor isomer appear at

δ10.95, δ5.69 and δ1.0- δ1.4 respectively. The above inferences can be collected together in the form of Scheme (IV-7) indicating the pterin ligand anion; supporting the inference from IR data. An octahedral coordination around the Mo(IV) atom involving three bidentated O,N donors as shown in Scheme (IV-3). The deshielding of the NH(8) signal is in line with the earlier observations on the Mo(IV) complex, reported in CHAPTER-III.

The 1-D and 2-D NMR data of H_2(mba) is represented in Fig. (IV-14) to Fig. (IV-16).

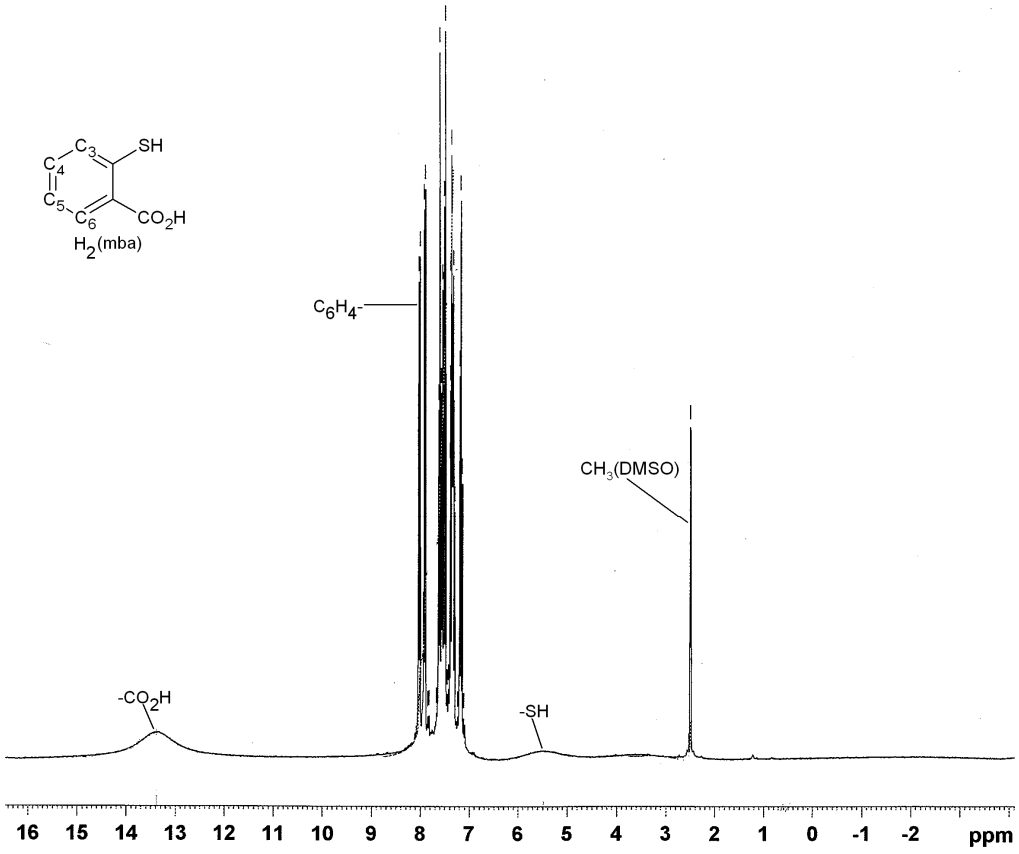

Fig. (IV-14): ^{1}H NMR data of H_2(mba) in DMSO-d_6 over the region δ16.0-0.0.

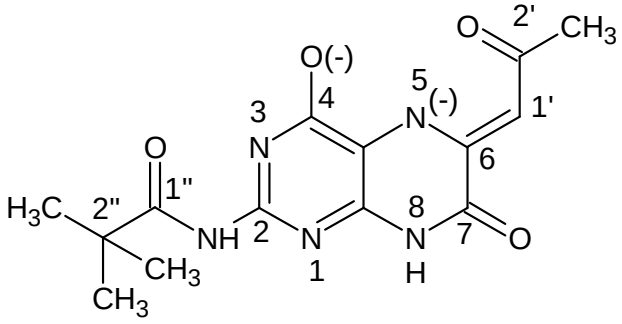

Scheme (IV-7)

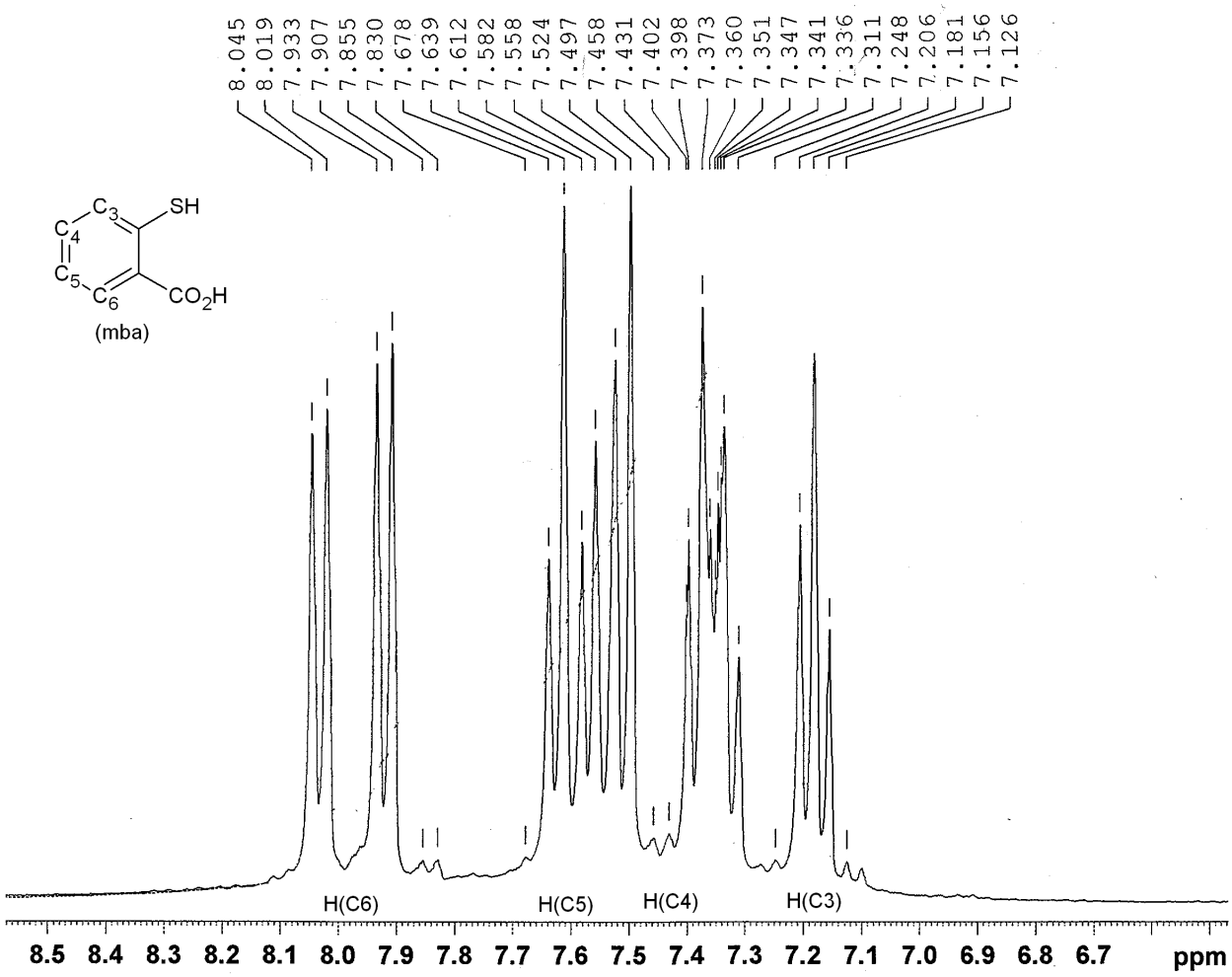

Fig. (IV-15): ^{1}H NMR data of H_2(mba) in DMSO-d_6 over the region δ8.5-6.7.

The 1-D and 2-D NMR data of **(2)** are presented in Fig. (III-17) to Fig. (III-19). The CH(1′), NH(2), CH_3(2′) [Scheme (IV-1)] and CH_3(2″) signals could be assigned at δ6.20, δ3.30, δ1.28 respectively. The NH(8) signals appears at δ12.30(wb); the OH(CH_3OH) signal is located at δ13.60. The CH(1′) and CH_3(2′) signals are undergo minor change from their free ligand position upon coordination to the [Mo(IV)] centre [Table (IV-2)]; non-participation of the 6-carbonyl group in the metal coordination process may be inferred. The strong deshielding of the NH(8) signal is due to participation of the O(4) atom in the coordination process, leading to electron density withdrawal from NH(8) position as par Joule's hypothesis [5b,c]. The O(4) atom along with the N(5) atom confers bidented pterin ligand coordination in this case. Besides this the NH(3) and NH(5) signals of the free ligand (H_2L^2) are absent here indicating their deprotonation during the metal coordination process. Taking into account the two CH_3OH molecules an overall coordination number of six is achieved here as indicated in Scheme (IV-4).

This NMR spectrum is characterized by a small amount of an additional isomer as indicated by the ^{1}H-NMR signal at δ3.39, δ6.05, δ7.45 and δ11.1 respectively. The aromatic ring protons of both $(Ph_4P)^{+}$ and $(mba)^{2-}$ appear at δ7.4- δ8.2, remaining essentially unchanged on coordination.

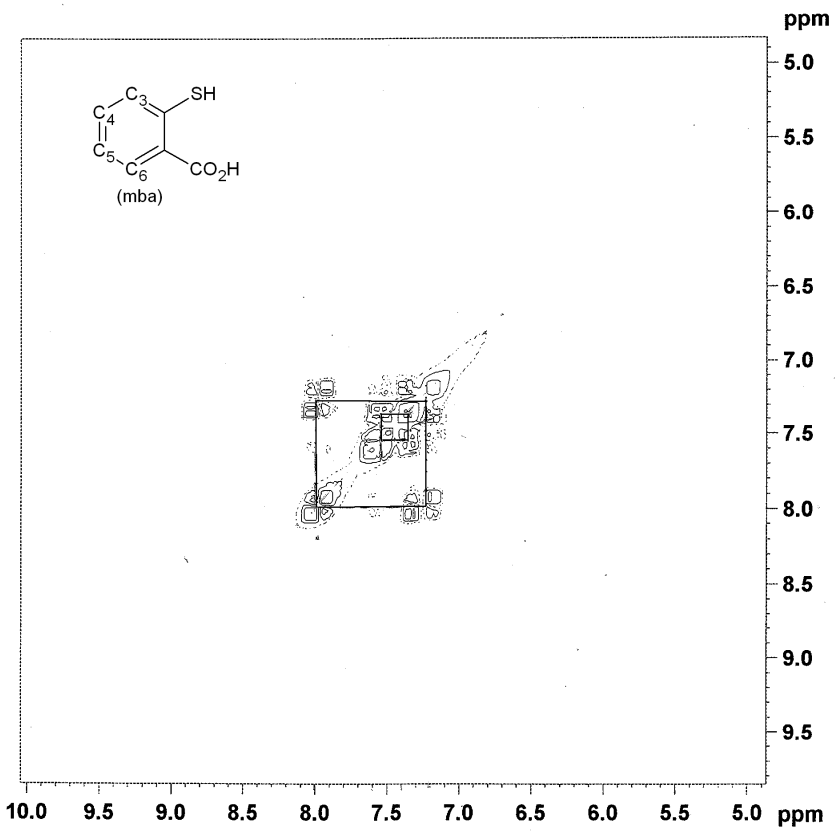

Fig. (IV-16): ^{1}H-^{1}H COSY data (symmetrized) of H_2(mba) in DMSO-d_6 over the region δ10.0-5.0.

^{1}H-NMR spectral data of **(3)** in DMSO-d_6 are shown in Fig. (IV-21) and Fig. (IV-22). Most of the 1D NMR signals [Fig. (IV-21)] have been assigned on the basis of the corresponding 2D NMR data [Fig. (IV-22)]. These results may be compared with those of [H_2L^2] [Fig. (III-19) and Fig. (III-20)] and [Na(dedtc).3H_2O] shown Fig. (IV-20).

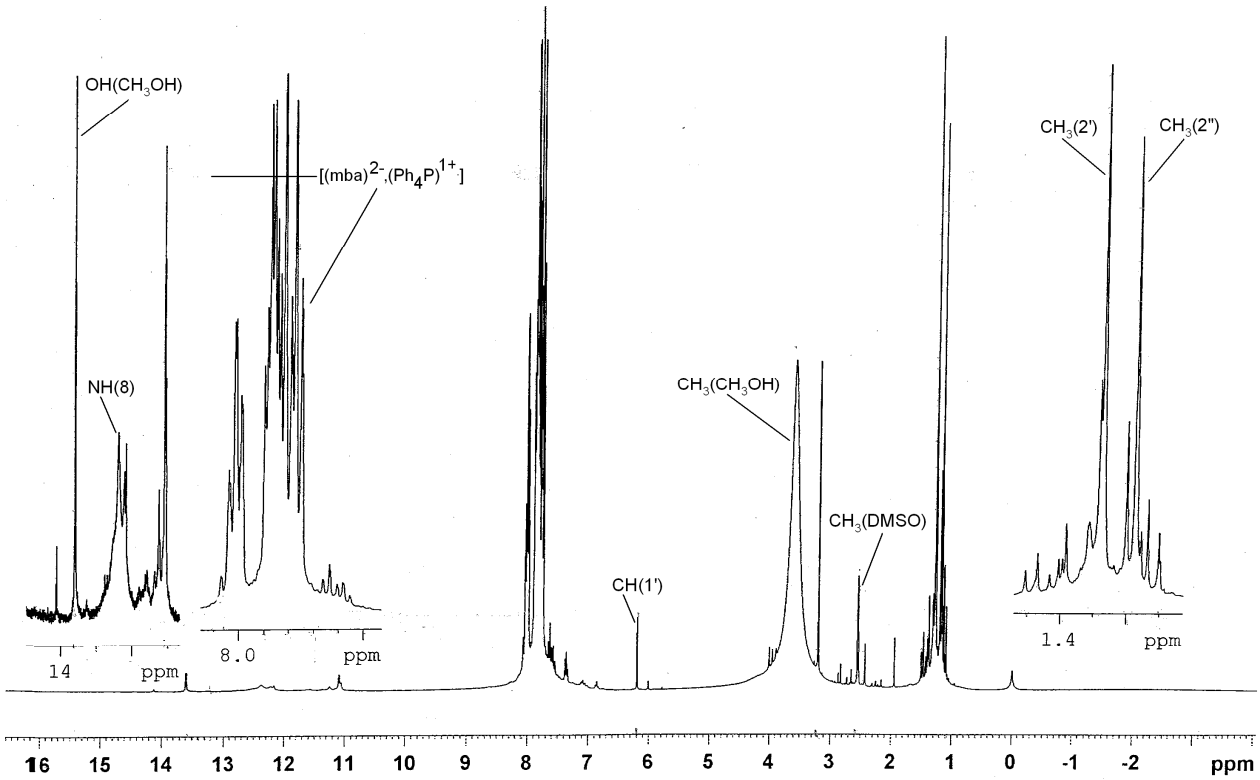

Fig. (IV-17): ^{1}H NMR data of compound **(2)** in DMSO-d_6 over the region δ16.0-0.0 (vide text for details).

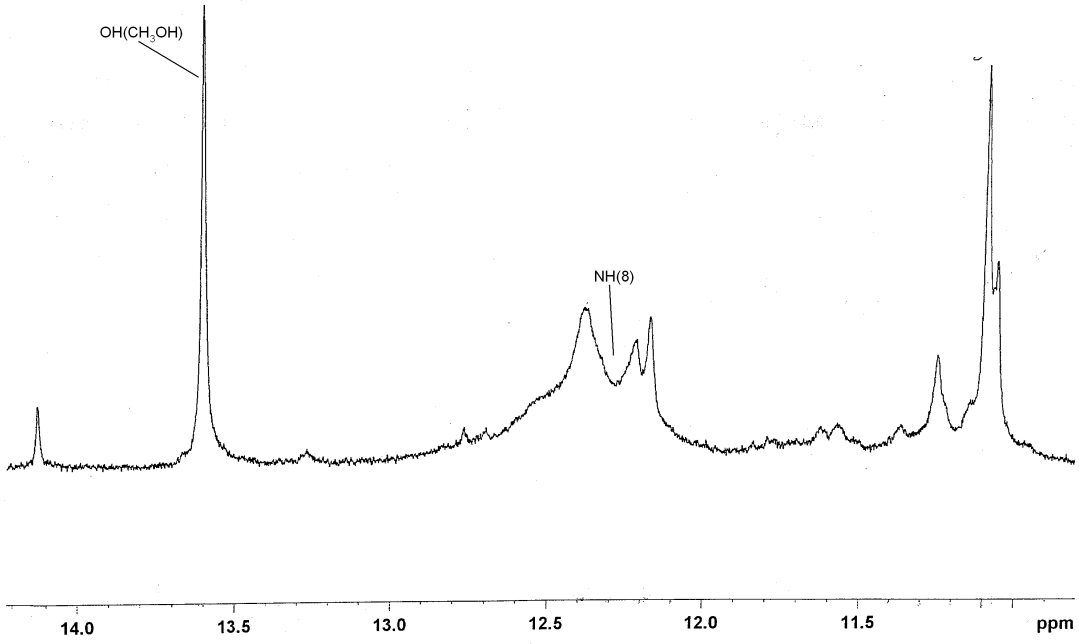

Fig. (IV-18): ^{1}H NMR data of compound **(2)** in DMSO-d_6 over the region δ14.0-11.0 (vide text for details).

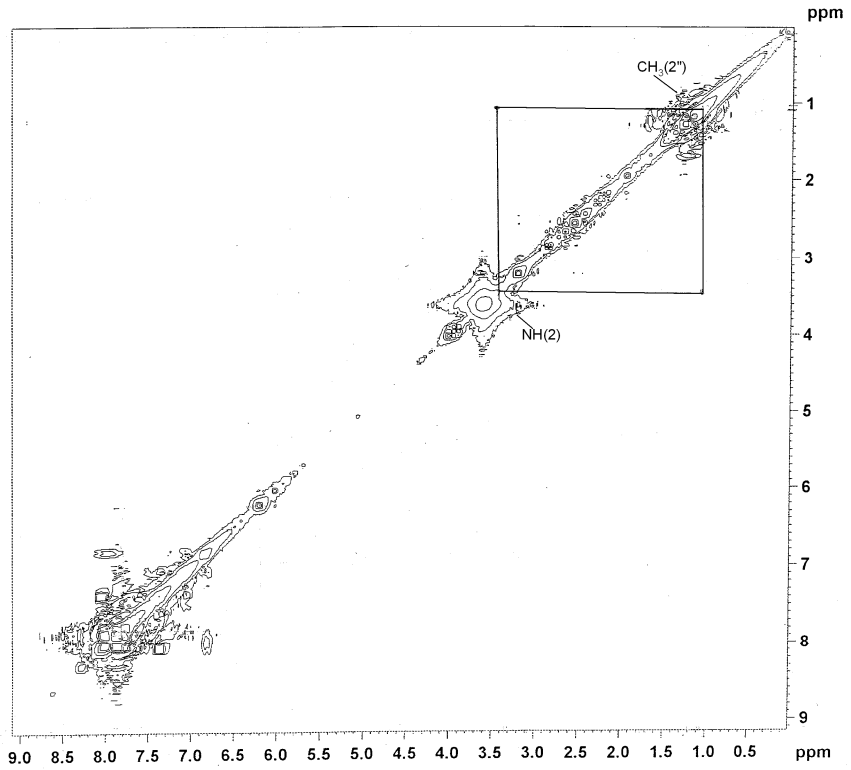

Fig. (IV-19): ^{1}H-^{1}H COSY data (symmetrized) of compound **(2)** in DMSO-d_6 over the region δ9.0-0.0 (vide text for details).

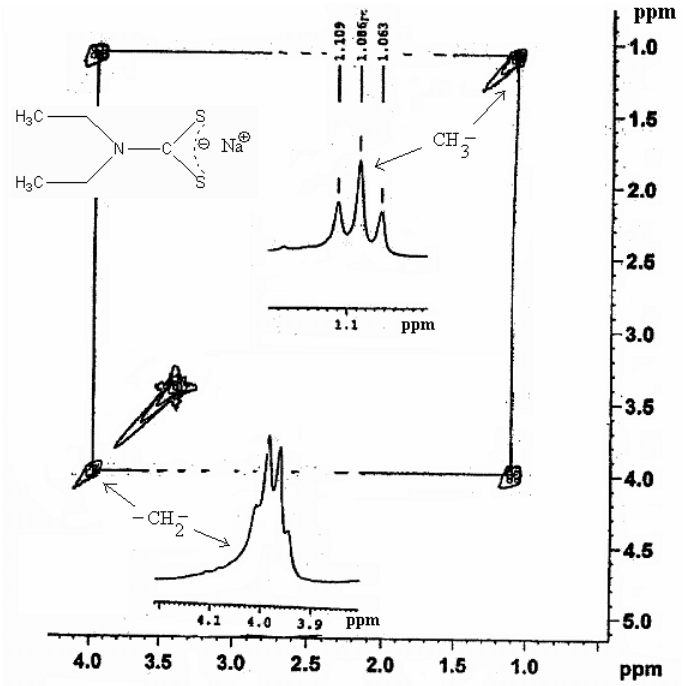

Fig. (IV-20): ^{1}H-^{1}H COSY data (symmetrized) of Na(dedtc).$3H_2O$ in DMSO-d_6, showing assignments of the CH_3- and $–CH_2$- proton signals.

As indicated in [Fig.(IV-21)] the NH(8) signal of the two pterin ligand residues appear at δ12.30 and δ11.05 respectively, indicating small differences between them on the NMR time scale. The OH(CH_3OH) signal is observed at δ13.33(ss). Beside these, a series of weaker signals are observed over the region δ11.00- δ14.5 arising from smaller isomer/conformer of **(3)**. The corresponding 2D NMR data [Fig.(IV-22)] stands in good stead for the unambiguous assignments of the CH_3 and $-CH_2-$ signals of the $(dedtc)^{1-}$ residue at δ3.3 and δ4.0 respectively. In the corresponding free ligand [Fig.(IV-20)] such signals appear at δ1.086 and δ4.0 respectively. From the 2-D NMR spectrum [Fig.(IV-22)] the NH(2) signal of pterin ligand residue, $(L^2)^{2-}$, merges with CH_3 signal of $(dedtc)^{1-}$ residue and appear at δ3.3 where as the $CH_3(2'')$ and $CH_3(2')$ proton signal appear at δ1.3 and δ1.17 respectively.

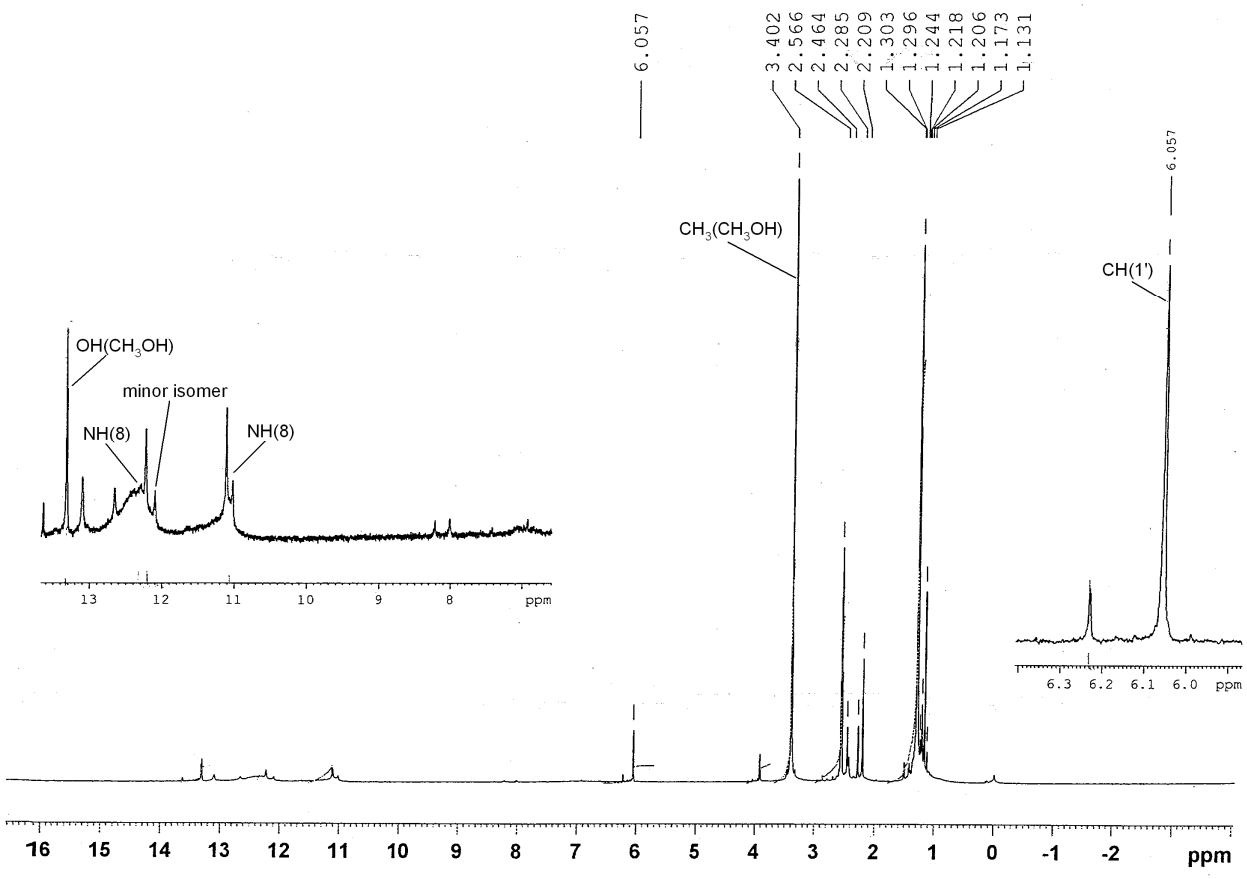

Fig. (IV-21): ^1H NMR data of compound **(3)** in DMSO-d_6 over the region δ16.0-0.0 (vide text for details).

The CH(1′) signal of $(L^2)^{2-}$ residue could be assigned at δ6.06 [Fig.(IV-21)]; it is associated with a weaker signal at δ6.23 assignable to a minor isomer, the major signal is hardly affected from its ligand position [Fig.(III-20)] at δ6.15, reflecting non-participation of the 2′

carbonyl group of the $(L^2)^{2-}$ residue in the complex formation process. That is, this pterin ligand acts as a bidented O,N donor through the O(4) and N(5) donor atoms as inferred from IR data. The signals of the $(dedtc)^{1-}$ residue are indicated in Fig. (IV-22).

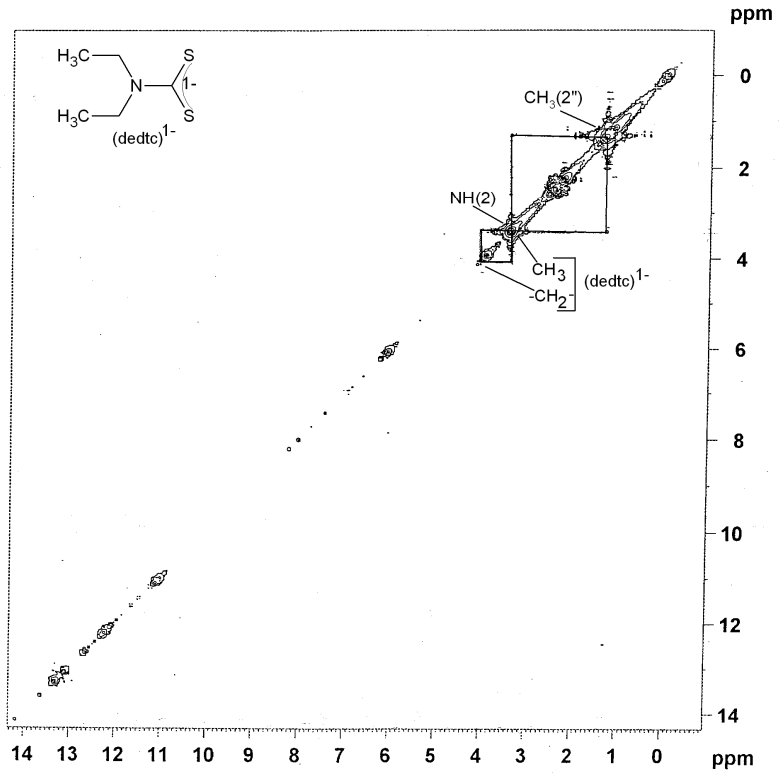

Fig. (IV-22): ^1H-^1H COSY data (symmetrized) of compound **(3)** in DMSO-d_6 over the region δ14.0-0.0 (vide text for details).

For compound **(4)** the 1-D and 2-D NMR spectra are represented by Fig. (IV-23) and Fig. (IV-24) respectively. Two sets of NH(8) signal of the pterin ligand residues $(L^2)^{2-}$ can be detected on NMR time scale, which appear at δ12.20(wb) and δ11.50(wb). The OH(CH_3OH) signal is observed at δ13.70(ss).The CH(1′) signals of two $(L^2)^{2-}$ residue could be assigned at δ6.20 and δ7.10 [Fig.(IV-23)]; they are associated with weaker signals at δ6.00 and δ6.98 assignable due to a minor isomer; the major signal is hardly affected from its ligand position [Fig.(III-20)] at δ6.15 reflecting non-participation of the 2′ carbonyl group $(L^2)^{2-}$ residues in the complex formation process. That is, these pterin ligands act as a bidented O,N donor through O(4) and N(5) donor atoms as inferred from IR data.

A closer look at the 2-D NMR spectrum [Fig. (IV-23)] of **(4)** reveals that two sets of NH(2) signal appear at δ3.45 and δ4.3. They are connected to two sets of CH_3(2″) as seen by off-diagonal peak at δ1.17 and δ1.33 respetively. The CH_3(2′) signals appear at δ1.21 and δ 1.30

respetively. The CH_3 and $–CH_2$- proton signal of ancillary ligand $(dedtc)^{1-}$ appear at δ3.20 and δ4.2 essentially unchanged to that of compound **(4)**.

Fluorescence spectra in CH_3OH

The change of electronic structure or coordination with respect to free ligand H_2L^2, may also be followed by fluorescence spectroscopy. The fluorescence spectraum of the compound **(1)** is presented in the Fig. (IV-25). From the Fig. (IV-25) it is found that the compound is of moderately fluorescent, as compared to the pterin ligand (H_2L^2) (non-fluorescent). This may be due to the gaining of aromaticity in the pyrimidine ring in the coordinated pterin ligand whereas the 1, 4 diazine ring remains nonaromatic [$(H_2L^2) \rightarrow (L^2)^{2-}$; Scheme (IV-1) and Scheme (IV-7)]. The λ_{max} were found at 420.5 nm and 479.5 respectively, reflects contribution from both the pterin and oxine ligand residues.

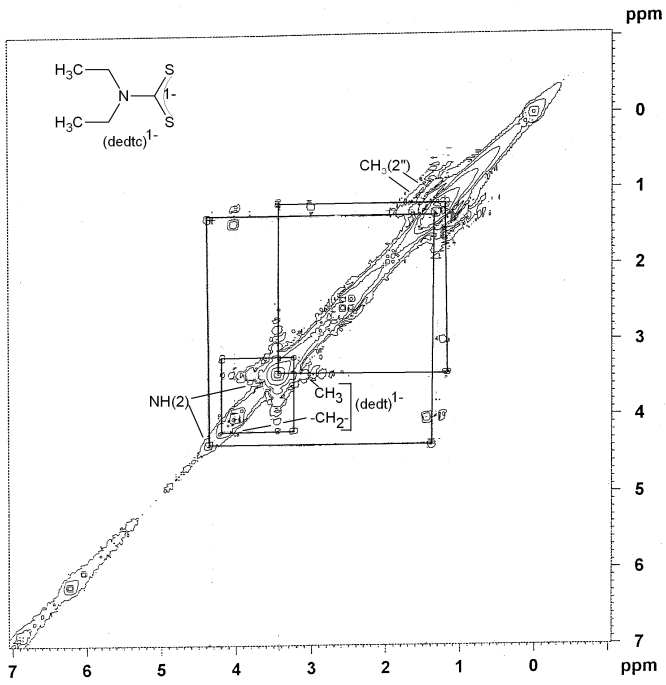

Fig. (IV-23): ^1H-^1H COSY data (symmetrized) of compound **(4)** in DMSO-d_6 over the region δ7.0-0.0 (vide text for details).

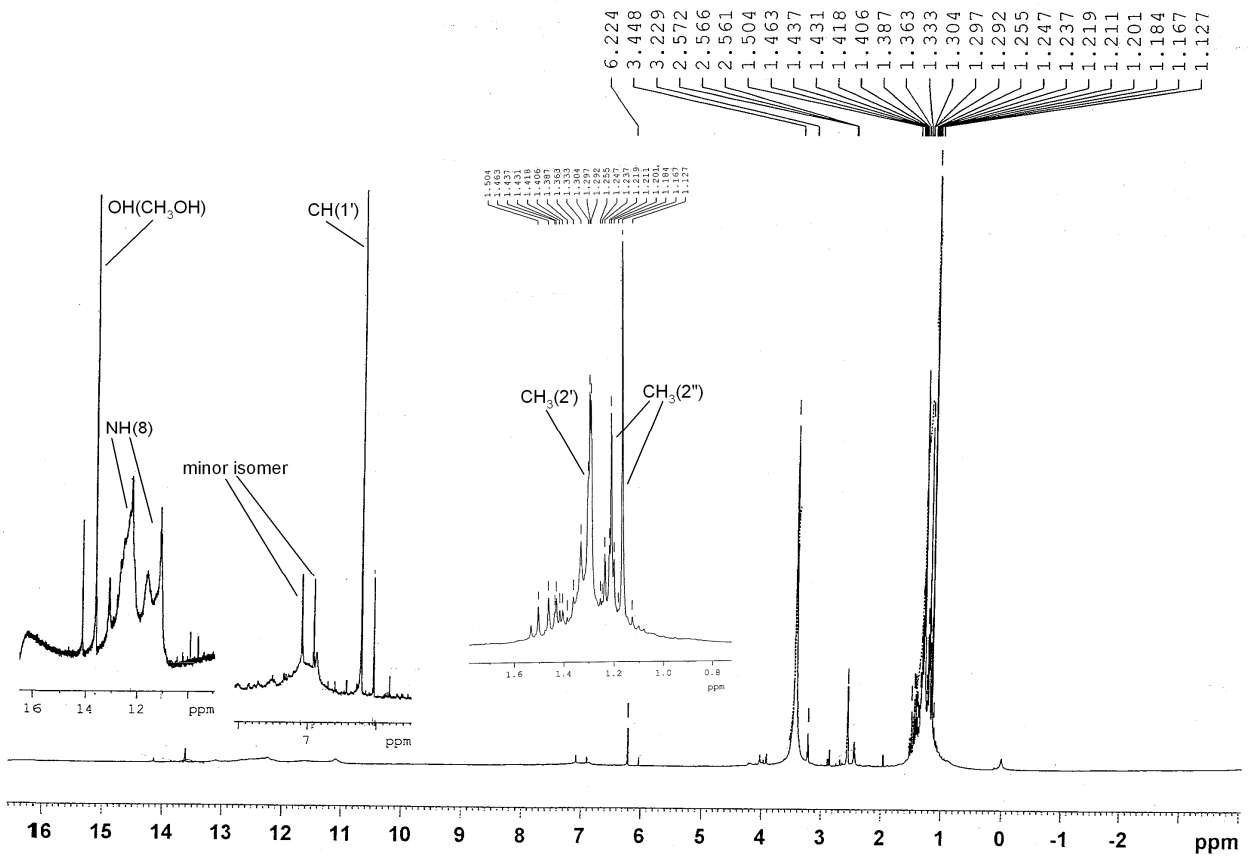

Fig. (IV-24): ^{1}H NMR data of compound **(4)** in DMSO-d_6 over the region δ16.0-0.0 (vide text for details).

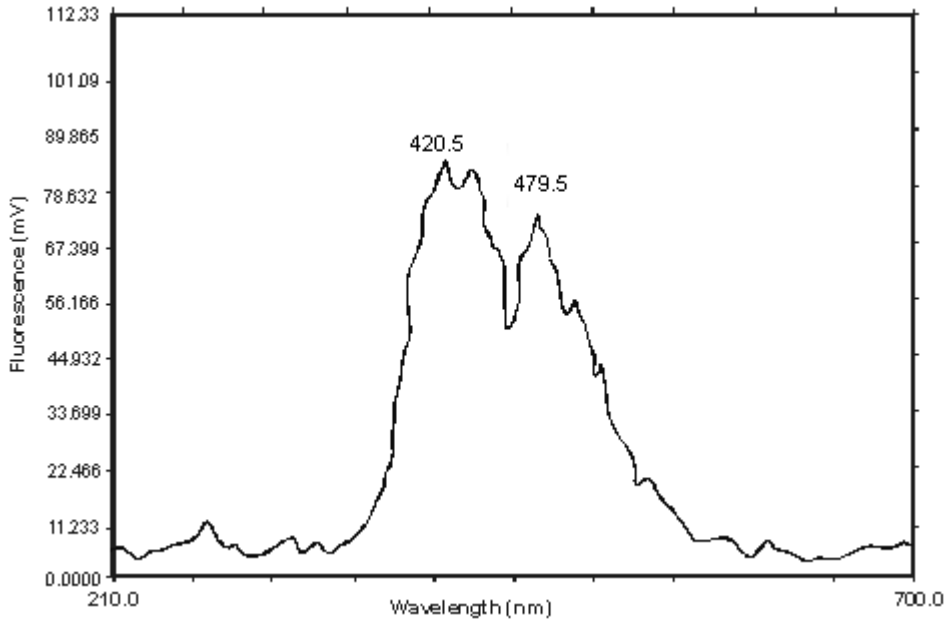

Fig. (IV-25): Fluorescence spectra in methanol of compound **(1)** (1.31×10^{-6} mol dm^{-3}).

Table (IV-2): Relevant ^{1}H-NMR signals in DMSO-d_6 (300 MHz, δ ppm, internal TMS) of the free ligand H_2L^2, the corresponding compounds (**1**) – (**4**) and Δ ($=\delta_{complex} - \delta_{ligand}$) values.

Compound [a]	$CH_3(2')(\delta)$ Δ*	$CH(1')(\delta)$ Δ*	$NH(8)(\delta)$ Δ*	$NH(2)(\delta)$ Δ*
(H_2L^2)	1.097	6.15	10.90	4.30
(1) [b]	1.11 0.013	6.12 -0.03	12.52 1.62	4.15 -0.15
(2) [b,c,d]	1.28 0.183	6.20 0.05	12.30 1.4	3.30 -1.0
(3) [b,c]	1.17 0.073	6.06 -0.09	12.30; 11.5 1.4; 0.6	3.30 -1.0
(4) [b,c]	1.21; 1.30 0.113;0.203	6.20; 7.10 0.05;0.95	12.20; 11.5 1.3; 0.6	3.45;4.30 0.85; 0.0

Abbreviations : ss = sharp singlet ; wb = weak broad.
[a]vide Scheme (IV-1) for the proton numbering system.
[b]CH_3OH signals of these complexes appear at δ 13.60 – 13.65 (-OH) and δ 3.41 – 3.40 (CH_3-) respectively.
[c]**the shielding of the NH(2) signal is associated with the electronic redistribution during complex formation process involving the redox non-innocent pterin ligand; concluding remarks of this thesis give a better picture**
[d]The phenyl ring proton signals of the Ph_4P^+ counter cation of **(2)**, appear at δ 8.0- δ 7.4. The 2D NMR data of PPh_4Br (in CH_3OH –d_4) is shown in Fig.(III-37).

In case of compound **(2)** the λ_{max} of the fluorescence spectrum [Fig. (IV-26)] is shifted to 479.5 nm due to contribution of the ancillary ligand, $(mba)^{2-}$.

In the fluorescence spectra of compound **(3)** [Fig. (IV-27)] a sharp increase in intensity was observed. The fluorescence property of the complex may be explained by the attainment of aromaticity by both the pterin residues. The λ_{max} appeared at 430.5 nm. The aliphatic backbone of the ancillary ligand [$(dedtc)^{1-}$] contributes to a lesser extent here at shorter wavelength region.

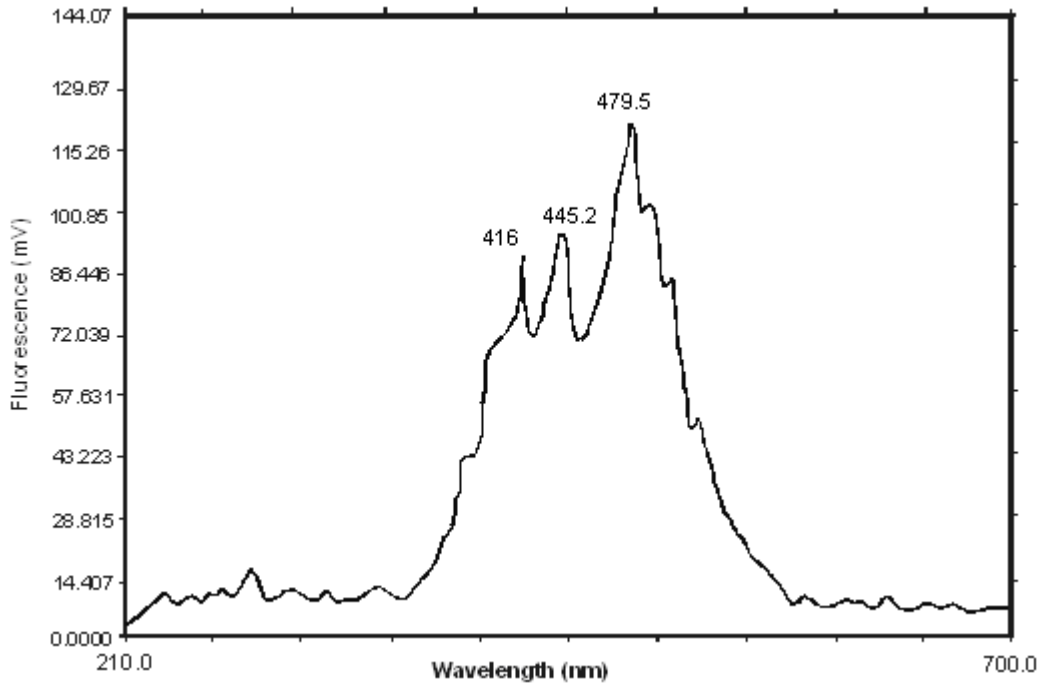

Fig. (IV-26): Fluorescence spectra in methanol of compound **(2)** (1.35×10^{-6} mol dm^{-3}).

F

or the compound **(4)** the fluorescence spectrum is presented in Fig. (IV-28). The intensity of this spectrum is lowered as compared to that in Fig. (IV-27) though the λ_{max} appears unchanged at 430.5 nm. It indicates that some electron density withdrawal has occurred from the pterin ring in this compound **(4)**, with two Mo(V) centers, as compared to that in compound **(3)** with a Mo(IV) center. That is, the florescence spectral data is able to follow the extent of metal-pterin interaction, in terms of the oxidation state of the metal center.

CHEM3D models

The above formulations were further substantiated by MM2 calculations to obtain a suitable CHEM3D models with lowest steric energies of these compounds [17,19]. For compound **(1)** one such model was obtained with lowest steric energy of 20.39 kcal/mol, Fig. (IV-29). This confirms the stability as well as geometry of the molecule. Some of the bond length and bond angle data of this compound obtained by MM2 calculations can be compared with literature values, as represented in the Table (IV-3).

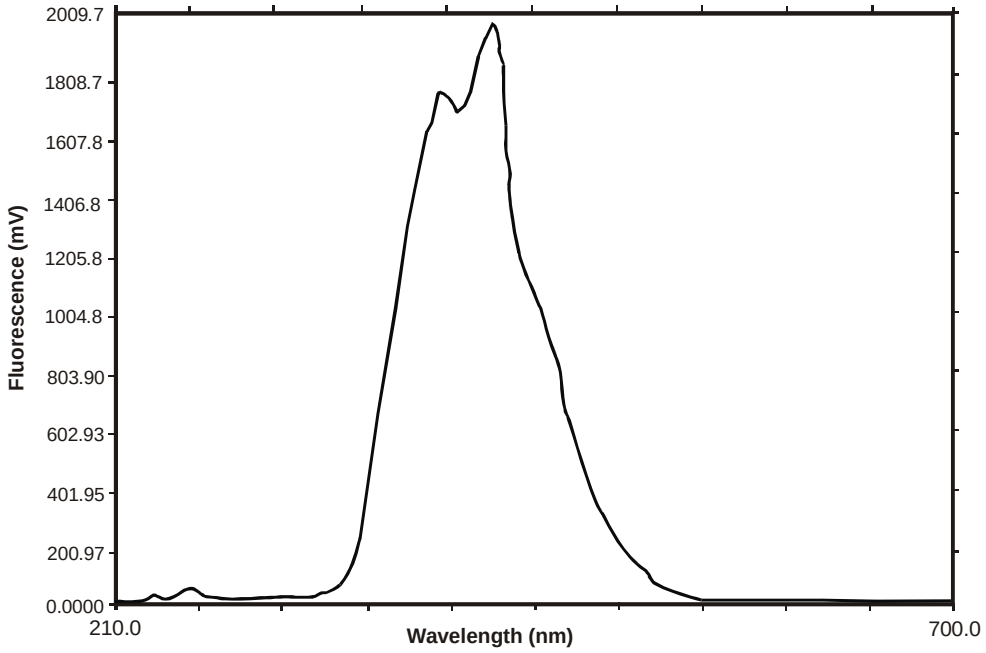

Fig. (IV-27): Fluorescence spectra in methanol of compound **(3)** (1.24×10^{-6} mol dm^{-3}).

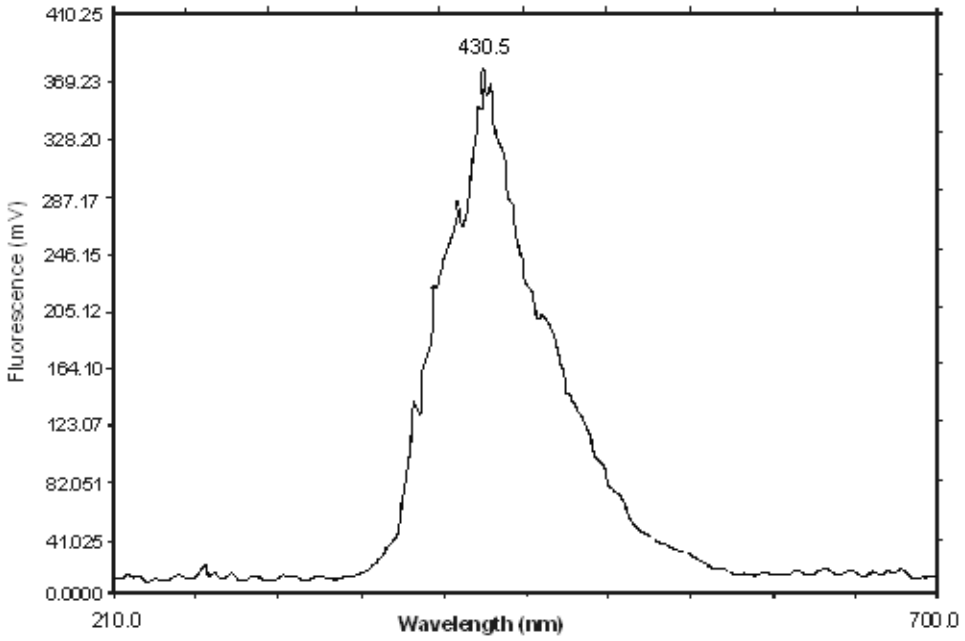

Fig. (IV-28): Fluorescence spectra in methanol of compound **(4)** (1.11×10^{-6} mol dm^{-3}).

Table (IV-3): Comparison of selected computed bond lengths (Å) and bond angles (deg) in compound **(1)** from the optimized geometry [Fig. (IV-29), MM2 calculations] with the available literature data (in parentheses) from x-ray structural studies*.

Bond distances (Å) [+]	bond angles (deg) [+,≠]
Mo(59)–O(10) 1.965	N(7) - Mo(33) - O(10)
(2.081-2.302)	85.46 (72 - 74)
Mo(59)–N(7) 1.997	O(10)-Mo(59)-O(63)
(1.997-2.080)	87.32 (93.5)
[±] Mo(59)–O(60) 1.964	O(60)-Mo(59)-O(63)
Mo(59)–O(63) 1.958	172.63 (158.0-169.2)
[±]Mo(59)–N(78) 1.997	O(63)-Mo(59)-N(78)
Mo(59) –N(59) 1.999	98.48 (92.1-98.8)

*X-ray structural data have been collected from the reference 1.

[+] Here O(10) and N(7) correspond to O(4) and N(5) donor atoms respectively, of the pterin ring as per Scheme (IV-1).

[±] Bond length data for the two $(ox)^{-1}$ ligand residues in compound **(1)**.

[≠]One set of selected bond angle data involving Mo(59) for compound **(1)**, is presented here.

Change of bond length data of the pterin ligand in this complex due to the coordination with the Mo atom may be a valuable guide to interpret the coordination mode of the ligand. Selected bond length data are compared and listed in the Table IV-4.

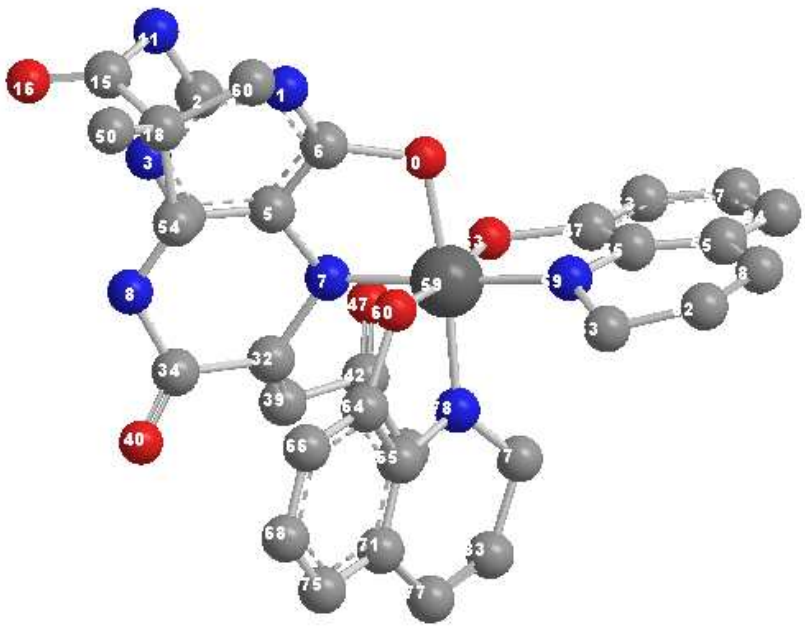

Fig. (IV-29): The optimized geometry (CHEM3D model obtained through MM2 calculations) of compound **(1)** with a steric energy of 20.39 kcal/mol.

Table (IV-4): Comparison of selected optimized bond lengths (Å) in the pterin ligand (H_2L^2) and the compound **(1)** from the respective optimized geometries (MM2 calculations).

Bond[+]	**H_2L^2**	**compound (1)**
N(3)-C(4)	1.446	1.335
C(4)-O(4)	1.234	1.561
N(5)-C(6)	1.282	1.595
C(6)-C(1')	1.512	1.327
C(6)-C(7)	1.707	1.710
C(7)-O(7)	1.219	1.211
C(7)-N(8)	1.551	1.448
C(2')-O(2')	1.214	1.215

[+] Scheme (IV-1) indicates the atom numbering system.

In case of compound **(2)** MM2 calculations was performed to obtain a CHEM3D model of lowest steric energy of 14.65 kcal/mol. Such a model is represented in the Fig. (IV-30). A slightly distorted octahedron around the Mo atom is observed. Comparison of some the bond length and bond angle data obtained from the MM2 calculation of this complex and with the available literature value are presented in the Table (IV-5).

From the Table (IV-5) it is evident that the Mo-N bond distance is fairly agree with that of literature value while the Mo-O(4) distances slightly shorter but comparable with Mo-O_b bond distance in Mo-O_b-Mo bond of binuclear complex. Table (IV-6) compares some of the optimized bond length data of free ligand (H_2L^2) and that of in this complex.

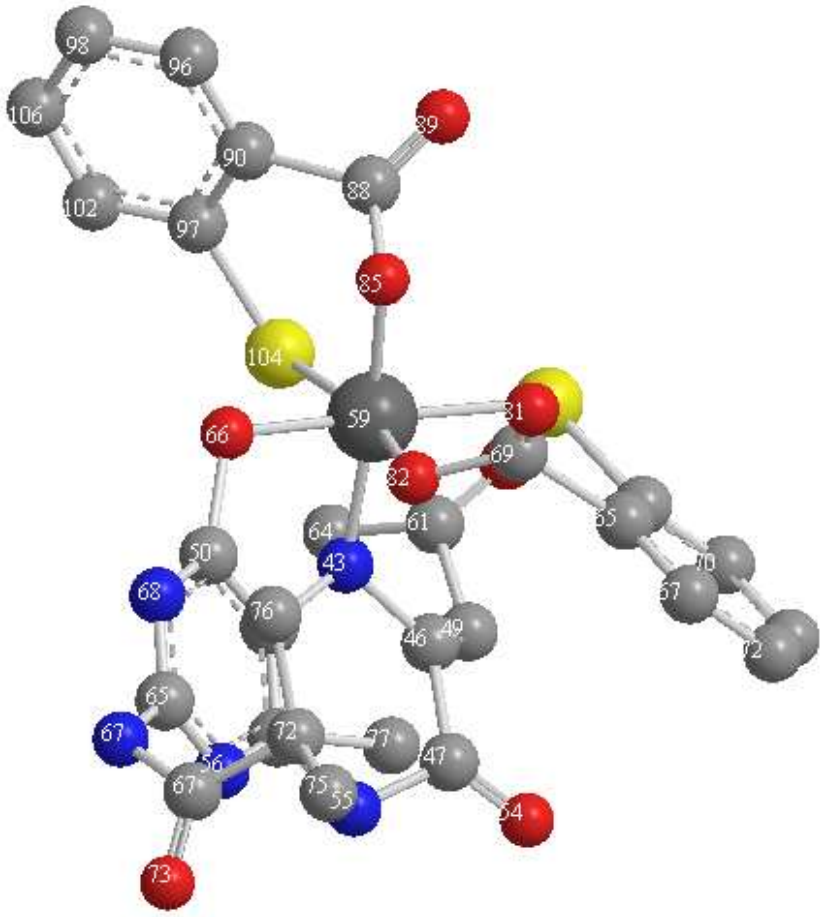

Fig. (IV-30): The optimized geometry (CHEM3D model obtained through MM2 calculations) of compound **(2)** with a steric energy of 14.65 kcal/mol.

Table (IV-5): Comparison of selected computed bond lengths (Å) and bond angles (deg) in compound **(2)** from the optimized geometry [Fig. (IV-30), MM2 calculations] with the available literature data (in parentheses) from X-ray structural studies*.

Bond distances (Å) [+]	bond angles (deg) [+,≠]
Mo(59) – O(66) 1.970	N(43) – Mo(59) – O(66)
(2.081-2.302)	84.79 (72 - 74)
Mo(59) – N(43) 2.003	S(99) – Mo(59) – S(104)
(1.997-2.080)	97.76 (83.69 – 96.9)
[±] Mo(59)–O(82) 1.966	
Mo(59)–O(85) 1.961	
[±] Mo(59) – S(99) 2.336	
Mo(59) – S(104) 2.338	
(2.393 – 2.360)	

*X-ray structural data have been collected from the reference 1.

[+] Here O(66) and N(43) correspond to O(4) and N(5) donor atoms respectively, of the pterin ring as per Scheme (IV-1).

[±] Bond length data for the two $(mba)^{-2}$ ligand residues in compound **(2)**.

[≠]One set of selected bond angle data involving Mo(59) for compound **(2)**, is presented here.

Table (IV-6): Comparison of selected optimized bond lengths (Å) in the pterin ligand (H_2L^2) and the compound **(2)** from the respective optimized geometries (MM2 calculations).

Bond [+]	**H_2L^2**	**compound (2)**
N(3)-C(4)	1.446	1.335
C(4)-O(4)	1.234	1.558
N(5)-C(6)	1.282	1.602
C(6)-C(1')	1.512	1.328
C(6)-C(7)	1.707	1.710

C(7)-O(7)	1.219	1.211
C(7)-N(8)	1.551	1.448
C(2')-O(2')	1.214	1.214

[+] Scheme (IV-1) indicates the atom numbering system.

The CHEM3D model [Fig. (IV-31)] shows the steric energy of 34.49 kcal/mol for compound **(3)**, unveiling both the stability and geometry of this complex. An octahedral geometry (slightly distorted) around the Mo atom is formed by the two oxygen atoms [namely O(10) and O(73)] and the two nitrogen atoms [namely N(7) and N(60)] and the two sulfur atoms [namely S(57) and S(98)]. Two basic parameters (namely bond length and bond angles) of this structure are compared with the literature data obtained through x-ray structural studies on different molybdenum pterin complex. This is shown in Table (IV-7).

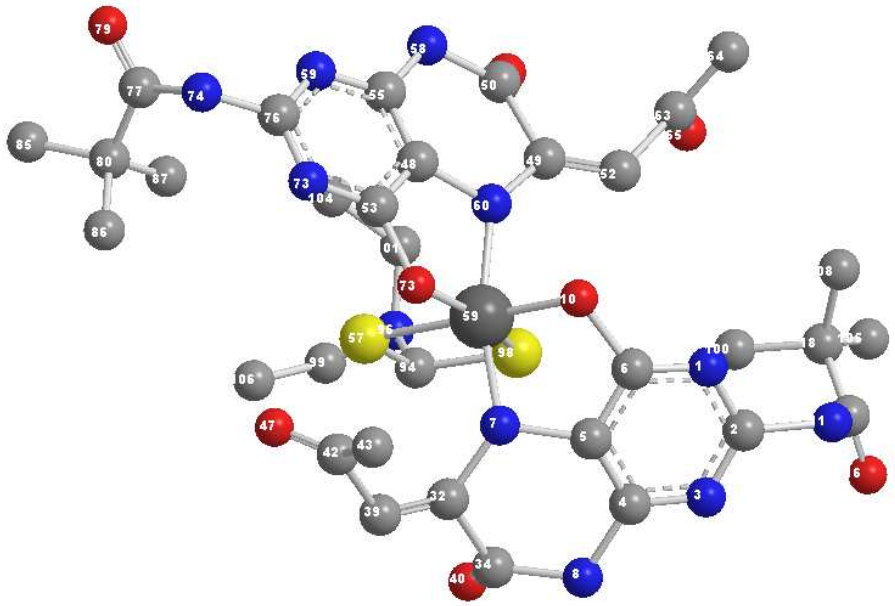

Fig. (IV-31): The optimized geometry (CHEM3D model obtained through MM2 calculations) of compound **(3)** with a steric energy of 34.49 kcal/mol.

Table (IV-7): Comparison of selected computed bond lengths (Å) and bond angles (deg) in compound **(3)** from the optimized geometry [Fig. IV-31, MM2 calculations] with the available literature data (in parentheses) from x-ray structural studies*.

Bond distances (Å) [+, †]	bond angles (deg) [+]
Mo(59)- O(10) 1.965	N(10) - Mo(33) - O(16)
Mo(59)- O(73) 1.964	82.43 (72 - 74)
(2.081-2.302)	
Mo(59)- N(7) 2.000	
Mo(59)- N(60) 1.995	
(1.997-2.080)	
Mo(59)- S(57) 2.362	
Mo (59)- S(98) 2.366	
(2.393 – 2.460)	

*X-ray structural data have been collected from reference 1.

[+] Here O(10), O(73) and N(7), N(60) correspond to O(4) and N(5) donor atoms respectively, of the pterin ring as per Scheme (IV-1).

[†] Bond length data for the two ligand residues in compound **(3)**.

Change of bond length data of the pterin ligand $(L^2)^{2-}$ residue in this complex from the free ligand (H_2L^2) values due to the coordination with the Mo atom, may be a valuable data to interpret the coordination mode of the ligand. Selected bond length data are compared and listed in the Table (IV-8).

A CHEM3D model of compound **(4)** giving a steric energy of 115.27 kcal/mol is presented as Fig. (IV-32). It may be noted that it is a binuclear di-μ-oxo complex. A comparison of some of the selected bond length and bond angle data (with literature values) is given in the following Table (IV-9).

Table (IV-8): Comparison of selected optimized bond lengths (Å) in the pterin ligand (H_2L^2) and the compound **(3)** from the respective optimized geometries (MM2 calculations).

Bond[+]	**H_2L^2**	**compound (3)**[±]
N(3)-C(4)	1.379	1.336,1.335
C(4)-O(4)	1.234	1.561,1.553
N(5)-C(6)	1.282	1.590,1.600
C(6)-C(1′)	1.512	1.328,1.327
C(6)-C(7)	1.707	1.718,1.721
C(7)-O(7)	1.219	1.213,1.213
C(7)-N(8)	1.551	1.575,1.578

[+] Scheme (IV-1) indicates the atom numbering system.

[±] Data for the two ligand residues in compound **(3)**.

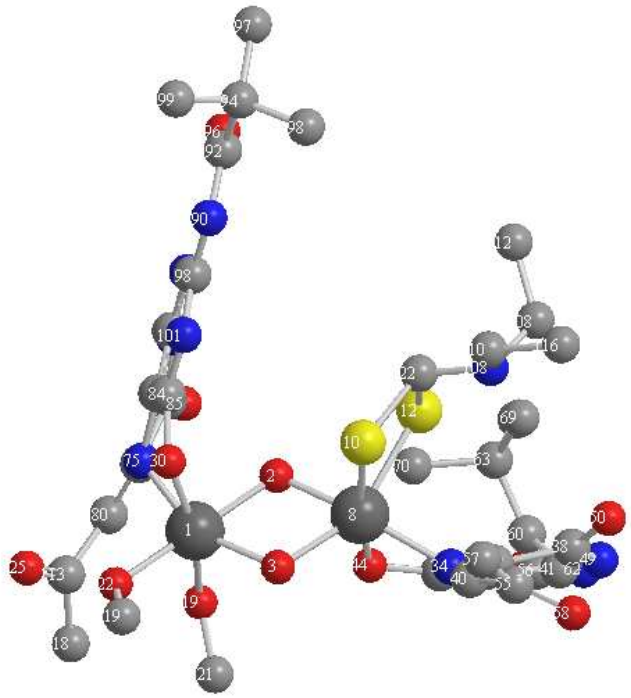

Fig. (IV-32): The optimized geometry (CHEM3D model obtained through MM2 calculations) of compound **(4)** with a steric energy of 115.27 kcal/mol.

Table (IV-9): Comparison of selected computed bond lengths (Å) and bond angles (deg) in compound **(4)** from the optimized geometry [Fig. (IV-32), MM2 calculations] with the available literature data (in parentheses) from X-ray structural studies*.

Bond distances (Å) [+]	bond angles (deg) [+]
Mo(1) - N(15) 1.990	N(75) - Mo(1) - O(30)
Mo(8) - N(100) 2.009	85.27 (72 - 74)
(1.997 - 2.080)	
Mo(1) - O(30) 1.996	
Mo(1) - O(115) 1.963	O(44) – Mo(8) – S(12)
Mo(1) - O(122) 1.960	113.94(92.2 – 94.8)
Mo(8) - O(44) 1.971	
(2.081 - 2.302)	
Mo(8) - S(10) 2.361	O(2) – Mo(1) – O(3)
Mo (8) - S(12) 2.364	70.72 (93.2)
(2.393-2.460)	
Mo(1) - O(2) 1.955	O(3) - Mo(1) - O(30)
Mo (1) - O(3) 1.958	97.23 (107.6)
Mo (8) - O(2) 1.964	
Mo (8) - O(3) 1.959	
(1.91 – 1.95)	

*X-ray structural data have been collected from the reference 1.

[+] Here O(30) and O(44) correspond to O(4), N(34) and N(75) correspond to N(5) and O(115) correspond to O(2') donor atoms, of the pterin ring as per Scheme (IV-1).

The bond length data of pterin ligand residue [$(L^2)^{2-}$] obtained from MM2 calculation are compared with the free ligand (H_2L^2) value and listed in Table (IV-10) below.

Table (IV-10): Comparison of selected optimized bond lengths (Å) in the pterin ligand (H_2L^2) and the compound **(4)** from the respective optimized geometries (MM2 calculations).

Bond[+]	**H_2L^2**	**compound (4)**[±]
N(3)-C(4)	1.379	1.334,1.336
C(4)-O(4)	1.234	1.543,1.559
N(5)-C(6)	1.282	1.604,1.580
C(6)-C(1′)	1.512	1.328,1.325
C(6)-C(7)	1.707	1.721,1.712
C(7)-O(7)	1.219	1.213,1.213
C(7)-N(8)	1.551	1.577,1.570
C(2')-O(2')	1.214	1.214,1.427

[+] Scheme (IV-1) indicates the atom numbering system.

[±]Data for the two pterin ligand [$(L^2)^{2-}$] residues in compound **(4)**.

It is evident from Tables (IV-4), (IV-6), (IV-8) and (IV-10) that on complex formation with the Mo atom here, a considerable change takes place in the pterin bond length data over the region from the N(3) atom to the C(1') atom. Schemes (IV-1) and (IV-7) help to visualize this aspect in terms of tautomerism/ deprotonation/coordination involving the process $H_2L^2 \rightarrow (L^2)^{2-} + 2H^+$. Thus these theoretical models (CHEM3D) provide with a suitable framework for discussion of the corresponding observed changes in IR, ^{1}H-NMR and fluorescence spectral data, as above. Bidentate pterin coordination [$(L^2)^{2-}$] through the O(4), N(5) atoms can be inferred in these coordination cores.

Compound **(1)**	Compound **(2)**
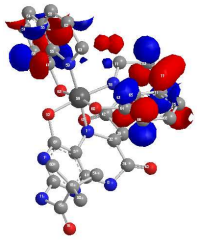	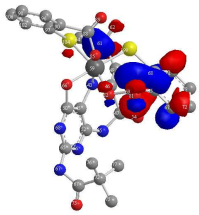
E_4(LUMO+1)= -2.456	E_4(LUMO+1)= -2.608
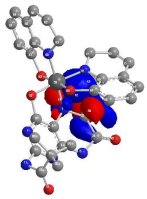	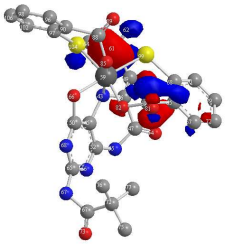
E_3(LUMO)= -3.289	E_3(LUMO)= -2.691
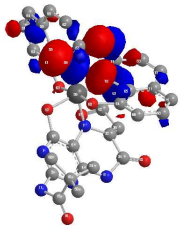	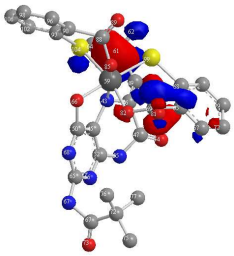
E_2(HOMO)= -8.728	E_2(HOMO)= -8.403
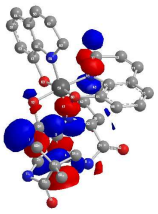	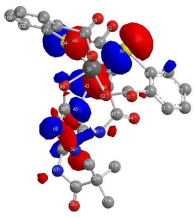
E_1(HOMO-1)= -9.249	E_1(HOMO-1)= -9.159
$\Delta(E_2-E_1)$ = 0.521 eV	$\Delta(E_2-E_1)$ = 0.756eV
$\Delta(E_3-E_2)$ = 5.439 eV	$\Delta(E_3-E_2)$ = 5.712 eV
$\Delta(E_4-E_3)$ = 0.833 eV	$\Delta(E_4-E_3)$ = 0.083 eV

Fig.(IV-33): The visualized frontier orbitals with energies (E, eV) of **(1)** and **(2)** (using Chem Office 2004, version 8.0).

Compound **(3)**	Compound **(4)**
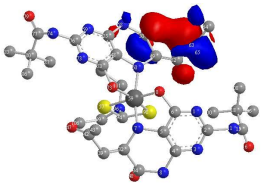	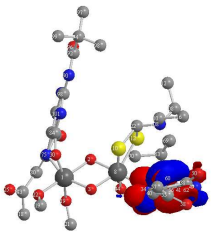
E_4(LUMO+1)= -2.664	E_4(LUMO+1)= -2.897
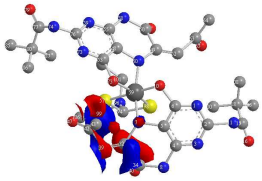	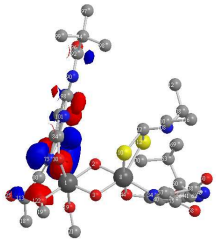
E_3(LUMO)= -2.898	E_3(LUMO)= -3.091
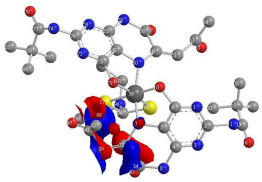	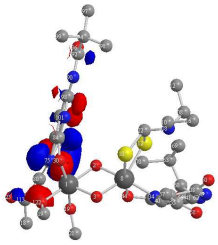
E_2(HOMO)= -5.931	E_2(HOMO)= -6.138
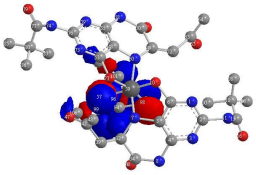	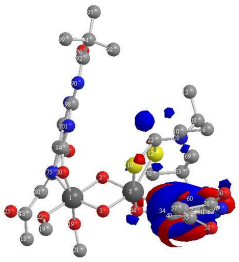
E_1(HOMO-1)= -7.885	E_1(HOMO-1)= -8.493
$\Delta(E_2-E_1)$ = 1.954 eV	$\Delta(E_2-E_1)$ = 2.355eV
$\Delta(E_3-E_2)$ = 3.033 eV	$\Delta(E_3-E_2)$ = 3.047 eV
$\Delta(E_4-E_3)$ = 0.234 eV	$\Delta(E_4-E_3)$ = 0.194 eV

Fig.(IV-34): The visualized frontier orbitals with energies (E, eV) of **(3)** and **(4)** (using Chem Office 2004, version 8.0).

The visualized frontier orbitals with energies (eV) of the complexes

Such data (extended Huckel surfaces) for the present complexes have been obtained, utilizing their CHEM3D models [17,19]. They are shown in Fig. (IV-33) and Fig. (VI-34). Some of the band gap data are helpful in rationalizing their chemical reativities, as discussed later.

UV-VIS spectroscopy in CH_3OH

The free pterin ligand (H_2L^2) absorbs at 294 nm due to ($\pi\rightarrow\pi^*$) transition.

For compound **(1)** the intraligand ($\pi\rightarrow\pi^*$) transition occurs at 281 nm. The absorption bands at 370 nm and 413 nm with large molar extinction coefficient values, are assigned to [L→Mo(IV)] type charge transfer transitions; they are responsible for the yellow-brown colour of this complex.

In case of compound **(2)** the intraligand ($\pi\rightarrow\pi^*$) transition occurs at 277 nm; the [L→Mo(IV)] type charge transfer transitions with large ε values occur at 346 nm and 418 nm (br, sh) respectively; they impart the deep brown colour to this complex.

For the snuff coloured compound **(3)** the intraligand ($\pi\rightarrow\pi^*$) transition and the charge transfer transitions, [L→Mo(IV)] type, are observed at 285 nm and 345 nm, 413 nm respectively. In case of compound **(4)** the corresponding transition occur at 288.5 nm and 347 nm, 421 nm respectively. The last two bands give rise to a dark brown colour for this complex.

Compounds **(1)** to **(3)** possess Mo(IV) centers which correspond to spin-paired d^2 centers. Compound **(4)** is a di-μ-oxo bridged Mo(V) system with two d^1 centers; the two electrons are in a spin-paired state, through the intervening oxygen atoms. The associated ‘d-d’ transitions of these compounds [**(1)** to **(4)**] are covered by the aforesaid CT transitions.

Reactivity study (in CH_3OH)

For the compound **(1)** its reactivity towards an enzyme substrate like Me_3NO was studied. The spectrophotometric monitoring of this reaction at 318K in CH_3OH is presented in the Fig. (IV-35). It can be noted that a gradual decrease in optical density from 265 mm to 460 mm. No definite isosbestic point is observed in the spectrum hinting the presence of intermediates [7]. An oxidation state of IV for the Mo center in this complex can be inferred.

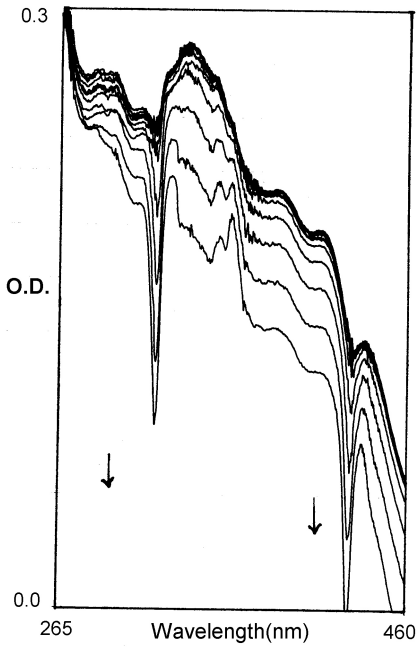

Fig. (IV-35): Absorption spectral changes recorded at 10 min interval during the reaction of compound **(1)** (0.7×10^{-5} mol) with $Me_3N \rightarrow O$ (3.46×10^{-3} mol) in CH_3OH at 318K.

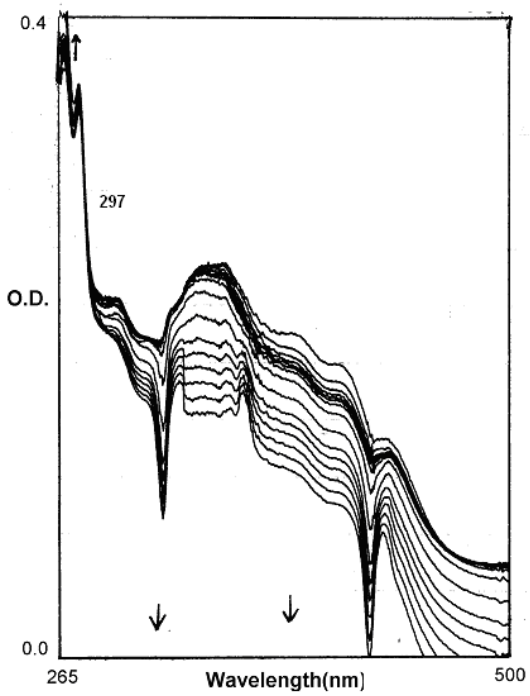

Fig. (IV-36): Absorption spectral changes recorded at 10 min interval during the reaction of compound **(2)** (8.57×10^{-5} mol) with $Me_3N \rightarrow O$ (3.46×10^{-3} mol) in CH_3OH at 319K.

Similar observation was also noted for the compound **(2)**. The complex was found to be reactive towards $Me_3N\rightarrow O$. The spectrophotometric monitoring of this reaction at 319K in CH_3OH is illustrated in the Fig. (IV-36). There is a continuous drop of optical density occurred in the region from 279 to 500 nm and increase in the opticaldensity in the region from 365-297 nm. A good isosbestic point is observed at 297 nm which falls in the intraligand ($\pi\rightarrow\pi^*$) region [7].

For the compound **(3)** a reaction with $Me_3N\rightarrow O$ in CH_3OH at 315K occurred. The spectrophotometric monitoring of the above reaction is presented in the Fig. (IV-37). A continuous decrease in optical density was observed at the region 280-500 nm.

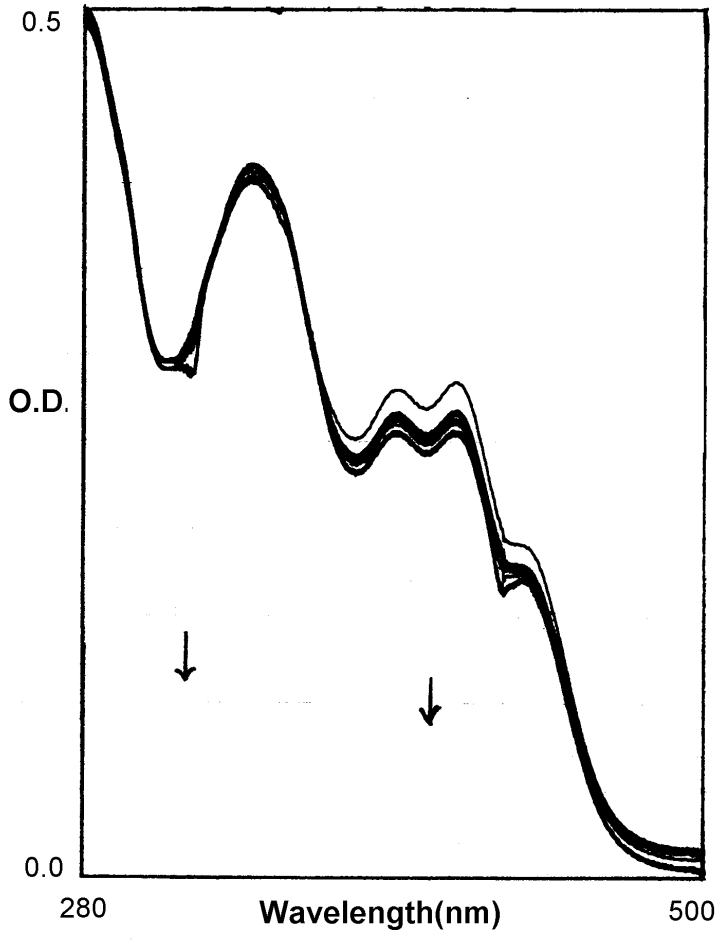

Fig. (IV-37): Absorption spectral changes recorded at 10 min interval during the reaction of compound **(3)** (1.66×10^{-5} mol) with $Me_3N\rightarrow O$ (2.66×10^{-3} mol) in CH_3OH at 315K.

The stoichiometry of the above reaction was studied and presented below. A solution of compound **(3)** (0.055 g, 0.06 mmol) in CH_3OH (60 mL) was stirred (in the dark) with $Me_3N{\rightarrow}O$ (0.0045 g, 0.06 mmol) for 60h (first 24h at 302K and the rest period at 313K); the gaseous product of the reaction, i.e., Me_3N (b.p. 275K) was driven off under a gentle flow of dry dinitrogen gas over the entire period into another flask containing a measured excess of perchloric acid in glacial acetic acid and the carrier gas escaped to the atmosphere through a silicone oil bubbler. Finally, the residual excess of perchloric acid was back titrated using a standard sodium acetate solution. For two moles of compound **(3)** added, ca. 0.80 mol of Me_3N was recovered, indicating a reaction represented by the Equation (IV-1a).

2 Compound **(3)** + $Me_3N{\rightarrow}O \rightleftharpoons$ [2 Compound **(3)**.$Me_3N{\rightarrow}O$] $\longrightarrow$

Me_3N + μ-oxo-Mo(V) complex …….[Equation (IV-1a)]

Traces of moisture present in the solvent (CH_3OH) ultimately affords to a di-μ-oxo Mo(V) complex [compound **(4)**] [Scheme (IV-6)] as the final product [Equation (IV-1b)].

μ-oxo Mo(V) complex + H_2O $\longrightarrow$ di-μ-oxo Mo(V) complex + $2H^+$

…….[Equation (IV-1b)]

The above multi step reaction pathway involving an associated type reaction intermediate, justifies the absence of isosbestic points in Fig. (IV-35), (IV-36) and (IV-37), especially in the L→Mo charge transfer region (340 – 430 nm).

Compound **(4)** was found to be reactive towards PPh_3 indicating abstraction of the bridging oxygen atom [Scheme (IV-6)]. A spectrophotometric monitoring of the reaction in CH_3OH at 322K is represented in the Fig. (IV-38). A continuous increase of optical density from wavelength 310-500 nm is observed. No isosbestic point was observed, indicating the presence of intermediate steps here as well.

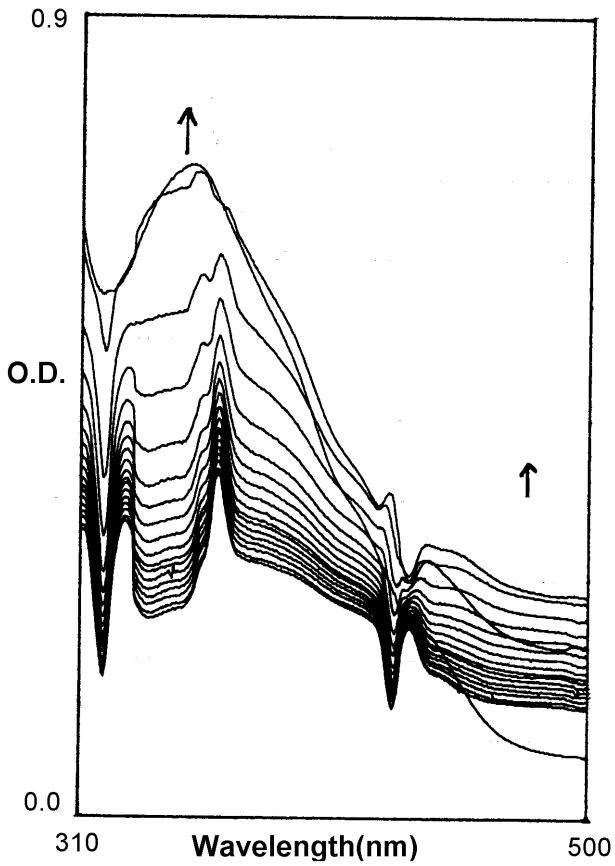

Fig. (IV-38): Absorption spectral changes recorded at 10 min interval during the reaction of compound **(4)** (2.22×10^{-5} mol) with PPh_3 (1.13×10^{-3} mol) in CH_3OH at 322K.

Cyclic voltametry (in DMF)

The cyclic voltammetric data of the free ligand (H_2L^2) is characterized by a single irreversible reduction peak at -0.93V. For compound **(1)** [Fig. (IV-39)] an irreversible metal centered reduction [Mo(IV) → Mo(III)] is observed at -0.73V. The two reduction peaks at -1.0V and -1.40V are ligand centered processes, with the later corresponding to the ancillary ligand residue, $(ox)^{1-}$. A reoxidation peak becomes apparent at faster scan rate, most likely associated with the ligand anion.

In case of compound **(2)** [Fig. (IV-40)] the metal centered reduction [Mo(IV) → Mo(III)] peak is observed at -0.9V. A peak at -1.62V corresponds to ligand centered reduction process.

In case compound **(3)** [Fig. (IV-41)] the metal centered reduction peak [Mo(IV) → Mo(III)] is observed at -0.6V. At faster scan rates this peak is not observed as they have been recorded later; solvent attack decomposes the original compound during the time interval.

Compound **(4)** with its Mo(V) centers present with an interesting case [Fig. (IV-42)]. Here the [Mo(V) → Mo(IV)] reduction peak is observed at -0.4V at slow san rate; it vanishes at higher scan rates due to the above-mentioned reason. The [Mo(IV) → Mo(III)] reduction occurs at -0.86V. The ligand centered reduction is observed at -1.50V. The cyclic voltammogram helps to follow the intermediate oxidation states, i.e., Mo(IV) on the cyclic voltammetric time scale. This highlights the efficacy of cyclic voltammetry, a temporal method, in identifying the reaction intermediate.

Among the above cyclic voltammograms, that of compound **(1)** stands apart in terms of significant contribution from the reoxidation peak. Most likely the small (~0.5V) band gap between the HOMO and HOMO-1 levels in this case is responsible for this observation. Besides this the band gap between the LUMO and LUMO+1 levels is not large (~0.8V)

Conclusion

The foregoing discussion are summarized in Table (IV-11). This chapter highlights the interesting chemistry of four new molybdenum-pterin complexes; three of them [compounds **(1)** to **(3)**] have been obtained through a redox reaction between Mo(VI) starting material ($Na_2MoO_4.2H_2O$) and the pterin ligand (H_2L^2) [Scheme (IV-1)]. The present characterization data point towards the presence of a Mo(IV) center in these complexes. The pterin ligand is oxidized to an aromatic state [Scheme (IV-7)], as evident from fluorescence spectral data. Compound **(4)** has been obtained through an oxygen atom transfer reaction with Me_3NO with compound **(3)**; a di-μ-oxo bridged Mo(V) core characterizes compound **(4)**. Intimate role of the redox non-innocent pterin ligand is largely responsible for the facile change over among the three biologically relevant oxidation states of molybdenum (IV/V/VI) here. This aspect throws light on the importance of the pterin ligand in the biological system in general and in oxomolybdoenzymes in particular.

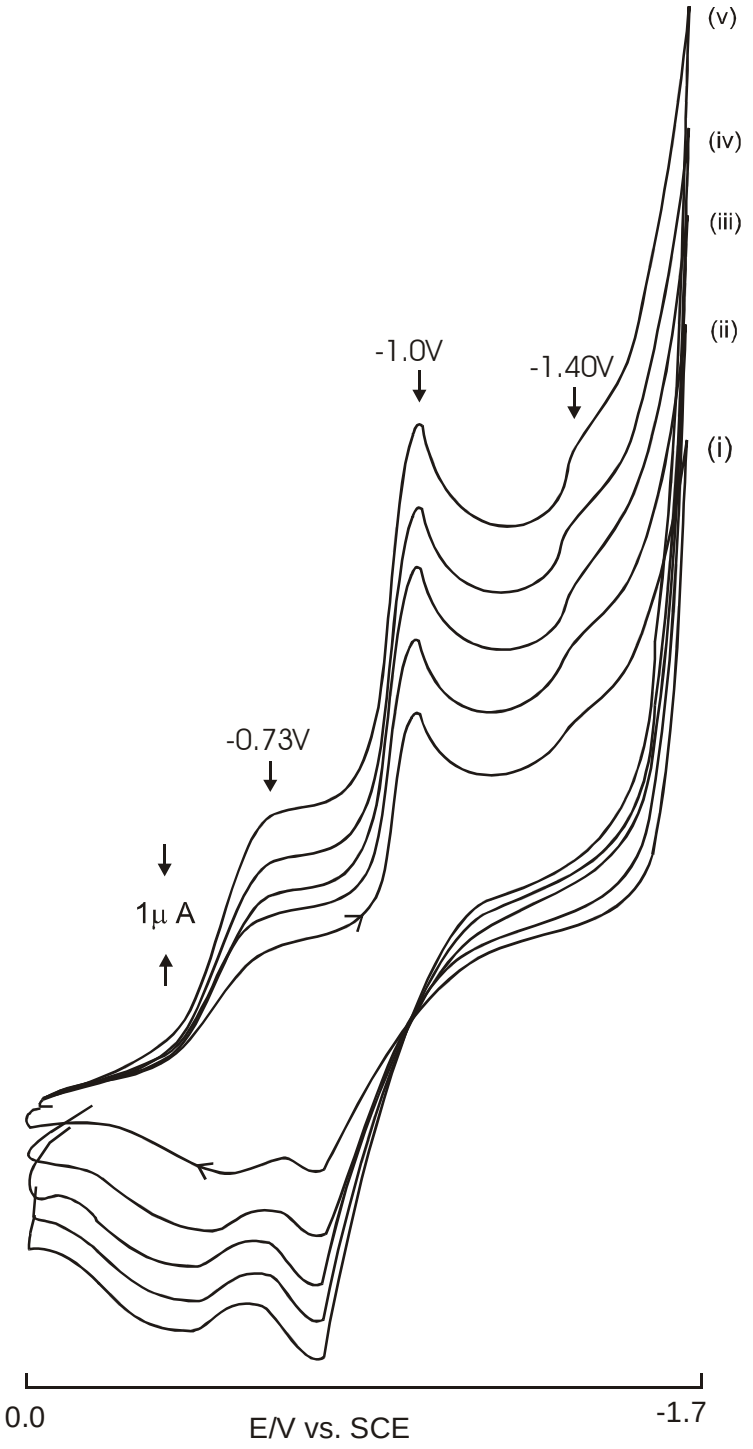

Fig. (IV-39): Cyclic voltammograms of the compound **(1)** (1.08×10^{-3} mol) in DMF (0.1 mol TBAP) at (i) 50 mVs^{-1}, (ii) 100 mVs^{-1}, (IV) 150 mVs^{-1}, (iv) 200 mVs^{-1} and (v) 250 mVs^{-1}.

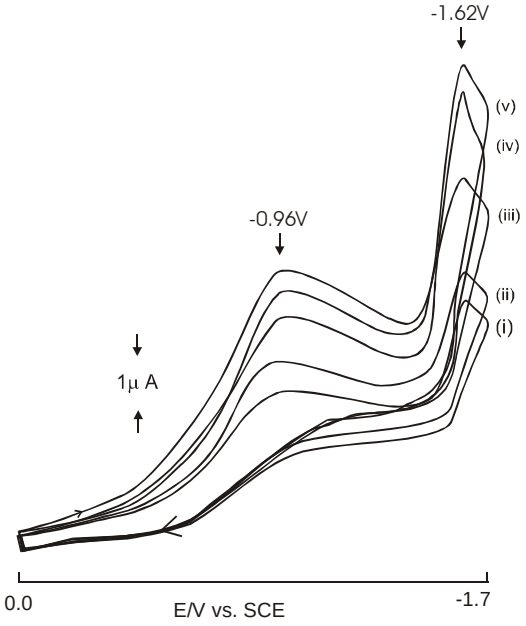

Fig. (IV-40): Cyclic voltammograms of the compound **(2)** (1.01 x 10^{-3} mol) in DMF (0.1 mol TBAP) at (i) 50 mVs^{-1}, (ii) 100 mVs^{-1}, (IV) 150 mVs^{-1}, (iv) 200 mVs^{-1} and (v) 250 mVs^{-1}.

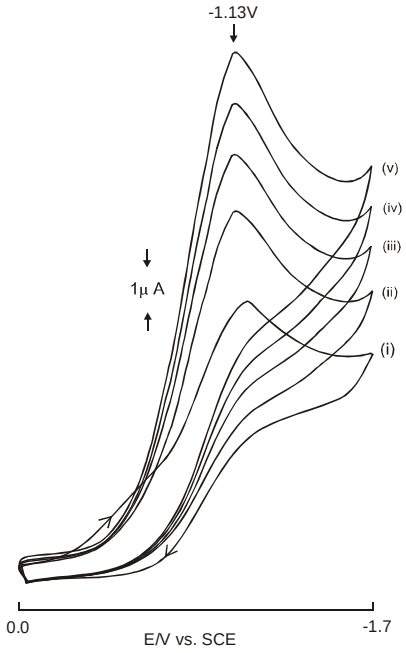

Fig. (IV-41): Cyclic voltammograms of the compound **(3)** (1.08 x 10^{-3} mol) in DMF (0.1 mol TBAP) at (i) 50 mVs^{-1}, (ii) 100 mVs^{-1}, (IV) 150 mVs^{-1}, (iv) 200 mVs^{-1} and (v) 250 mVs^{-1}.

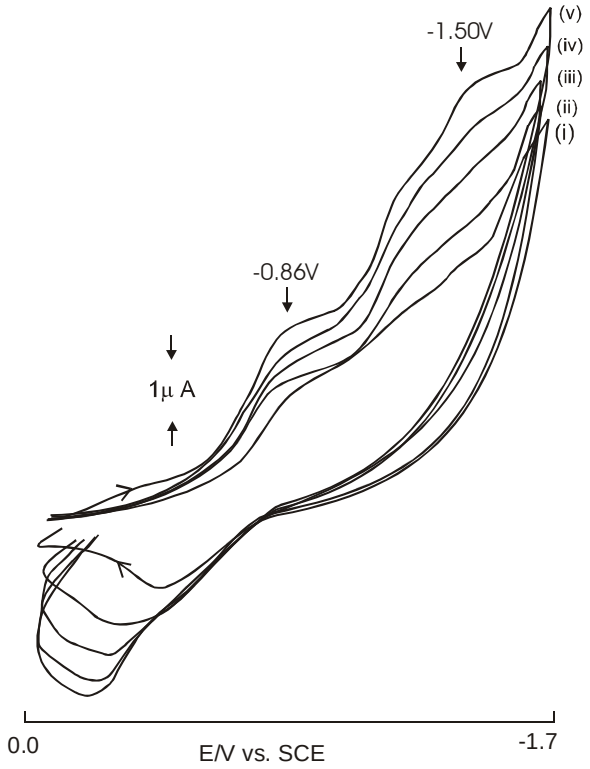

Fig. (IV-42): Cyclic voltammograms of the compound **(4)** (0.89 x 10^{-3} mol) in DMF (0.1 mol TBAP) at (i) 50 mVs^{-1}, (ii) 100 mVs^{-1}, (IV) 150 mVs^{-1}, (iv) 200 mVs^{-1} and (v) 250 mVs^{-1}.

CHEM3D models of these complexes provide with suitable reference point for interpreting their IR, ^{1}H-NMR and fluorescence spectral data. Reactivities of these compounds [**(1)** to **(3)**] towards Me_3NO helps to acertain an oxidation state of (IV) for the metal center in these cases. For establishing the reaction stoichiometry one of the products [compound **(4)**] of the above type reactivity has established and characterized. Such a step assisted in proposing mechanism for the oxygen atom transfer reaction involving an associative type intermediate. Cyclic voltammetric data are also helpful in characterizing these complexes including an intermediate oxiadation state for compound **(4)**. ^{1}H-NMR spectral data [Table (IV-2)] of compounds **(2)** and **(3)** are quite interesting. For example shielding of the NH(2) signal in these complexes can be correlated with the S→Mo electron transfer through suitable π – orbitals, eventually to the NH(2) group through the pterin ring pπ – orbitals. Concluding remarks of this thesis give a comprehensive view of this aspect.

Table (IV-11): Comparison of different physic-chemical parameters of the molybdenum compounds of the pterin ligand (H_2L^2) with selected ancillary ligands.

Compounds→ / Parameters ↓	Compound **(1)** of Chapter III	Compound **(1)**	Compound **(2)**	Compound **(3)**	Compound **(4)**
1. Colours	deep brown	yellow-brown	deep brown	snuff	dark brown
2.UV-VIS data	280(4.38), 346(4.69), 376sh(4.58), 415(4.48), 450sh(4.21).	218(4.96) 241(4.95) 281sh(4.48) 307sh(4.36) 346(4.51) 370sh(4.38) 413(4.33) 441sh(4.09)	223sh(5.07) 277sh(4.38) 346(4.11) 418sh(3.86) 449sh (3.66)	219(4.86), 242sh(4.52) 285sh(4.39) 345.5(4.39) 413.5(4.26) 443.0 sh(4.09)	217(5.08) 248.5sh (4.80) 288.5(4.75) 347(4.69) 421sh(4.35) 448sh (4.17)
3.Floures cense data (λ_{max}/ nm)	402	420.5	479.5	430.5	430.5
3. Steric energy (Kcal/mol)	69.37	20.39	14.66	34.49	51.32
4. Cyclic Voltammetry data [E_{pc}(V) of Mo(IV) →Mo(III)]	-0.98	-0.73	–0.9	–0.6	-0.4* and -0.86
5. Substrate for reactivity study	$Me_3N\rightarrow O$	$Me_3N\rightarrow O$	$Me_3N\rightarrow O$	$Me_3N\rightarrow O$	PPh_3
6. ΔE (HOMO-LUMO) eV	5.66	5.439	5.71	3.03	3.04

* Corresponds to Mo(V) → Mo(IV) reduction peak

CHEM3D models of these complexes provide with suitable reference point for interpreting their IR, ^{1}H-NMR and fluorescence spectral data. Reactivities of these compounds [**(1)** to **(3)**] towards Me_3NO helps to acertain an oxidation state of (IV) for

For compounds **(1)** and **(3)** almost intact molecular ion peak are observed in the ESIMS data [Fig. (IV-1), Fig. (IV-3); Table (IV-1)], indicating exceptional stability of these complexes.

At first it may appear unusual due to the presence of branched chains at the 2- and 6- positions of the pterin ligand [Scheme (IV-1)]. During the complex formation proess, an electronic redistribution occurs involving the entire pterin ligand, leading to the formation multiple bonds, holding the above branched chains [Scheme (IV-7)] especially for compound **(3)**. This once again highlights the redox non-innocent behaviour of the pterin ligand ($H_2L^2/(L_2)^{2-}$].